

# CholeskyQR with Randomization and Pivoting for Tall Matrices (CQRRPT)

Maksim Melnichenko\*      Oleg Balabanov<sup>†‡</sup>      Riley Murray<sup>§</sup>  
 James Demmel<sup>†</sup>      Michael W. Mahoney<sup>‡¶</sup>      Piotr Luszczek\*

February 6, 2024

## Abstract

This paper develops and analyzes a new algorithm for QR decomposition with column pivoting (QRCP) of rectangular matrices with large row counts. The algorithm combines methods from randomized numerical linear algebra in a particularly careful way in order to accelerate both pivot decisions for the input matrix *and* the process of decomposing the pivoted matrix into the QR form. The source of the latter acceleration is a use of randomized preconditioning and CholeskyQR. Comprehensive analysis is provided in both exact and finite-precision arithmetic to characterize the algorithm’s rank-revealing properties and its numerical stability granted probabilistic assumptions of the sketching operator. An implementation of the proposed algorithm is described and made available inside the open-source **RandLAPACK** library, which itself relies on **RandBLAS**—also available in open-source format. Experiments with this implementation on an Intel Xeon Gold 6248R CPU demonstrate order-of-magnitude speedups relative to LAPACK’s standard function for QRCP, and comparable performance to a specialized algorithm for unpivoted QR of tall matrices, which lacks the strong rank-revealing properties of the proposed method.

## 1 Introduction

The QR factorization, considered one of “The Big Six Matrix Factorizations” [Hig22], is fundamental to the field of numerical linear algebra. Its applications range from linear least squares problems [Bjö96] and block orthogonalization [SW02] to contemporary randomized low-rank approximation algorithms [TW23]. Beyond the basic QR decomposition, QR with column pivoting (QRCP) has additional benefits for numerically challenging problems, as it can help with rank-revealing tasks. To describe this problem concretely, let  $\mathbf{M}$  be a matrix of size  $m \times n$  with  $m \geq n$ . QRCP is concerned with finding a column permutation matrix  $\mathbf{P}$  and a QR decomposition of the product  $\mathbf{MP}$ , i.e.,

$$\mathbf{MP} = \mathbf{QR}$$

---

\*Innovative Computing Laboratory, University of Tennessee, Knoxville

<sup>†</sup>University of California, Berkeley

<sup>‡</sup>International Computer Science Institute (ICSI)

<sup>§</sup>Sandia National Laboratories

<sup>¶</sup>Lawrence Berkeley National Laboratory

Funding acknowledgments and additional affiliations appear at the end of the paper.

Send correspondence to the first three authors, at mmelnic1@vols.utk.edu, olegbalabanov@gmail.com, and rjmurr@sandia.gov, respectively.

such that the information on the leading and trailing singular values of  $\mathbf{M}$  can be inferred from the spectra of leading and trailing blocks in  $2 \times 2$  partitions of  $\mathbf{R}$ .

QRCP is considerably more expensive than unpivoted QR, even with straightforward pivoting strategies. For example, the leading-order term in the flop count for unpivoted QR using Householder reflectors (“Householder QR”) [BG65] is  $2mn^2$ , while the analogous term for Householder QR with max-norm column pivoting is  $4mn^2$  [GVL13, Algorithm 5.4.1]. The extra flops for the max-norm pivoting stem from the need to update the column norms of every partial decomposition of  $\mathbf{M}$  as the algorithm progresses from left to right across the columns. Critically, these column-norm updates entail Level 2 BLAS operations, which are less suitable for modern hardware than matrix-matrix products abundant in classic unpivoted QR. Level 2 operations are bound by the main memory bandwidth, making it impossible to reach the theoretical compute limit of any recent machine for matrices exceeding the size of the Level 1 cache [QOSB98]. Furthermore, they introduce an extensive number of inter-processor synchronizations, significantly impairing performance on distributed memory systems.

We use methods common in Randomized Numerical Linear Algebra (RandNLA) to develop a fast and reliable QRCP algorithm we call *CQRRPT*,<sup>1</sup> which stands for “CholeskyQR with Randomization and Pivoting for Tall matrices.” As we show below, CQRRPT can outperform not only other QRCP algorithms but also specialized communication avoiding algorithms for unpivoted QR, such as shifted CholeskyQR3 [FKN<sup>+</sup>20] and TSQR [DGHL12]. The dominant cost of our algorithm is attributed to three matrix-matrix operations (Level 3 BLAS) and a random projection, rendering it highly efficient from the communication standpoint. On distributed memory systems, it can be implemented with just two sum-reduce exchanges. Compared to shifted CholeskyQR3, CQRRPT requires  $\frac{4}{3} \times$  fewer data passes and  $\frac{3}{2} \times$  fewer inter-processor messages. Furthermore, compared to TSQR, CQRRPT lends itself more easily to performance optimization on massively parallel architectures, thanks to its simple reduction operator. The highly efficient computational profile, together with CQRRPT’s unconditional numerical stability, means that CQRRPT essentially “solves” the algorithm design problem of QRCP for tall matrices.

## 1.1 Random sketching

CQRRPT only uses randomness when sampling a linear dimension reduction map from a prescribed distribution. This happens only once, at the very beginning of the algorithm. The sampled linear map is called a *sketching operator*, which we say is sampled from a *sketching distribution*. The image of a data matrix under a sketching operator is called a *sketch*. Computing a sketch can be as simple as selecting rows from a matrix and as complicated as algorithmic variants for computing Fast Fourier Transforms. Our implementation of CQRRPT uses structured sparse sketching operators since these can provide exceptional speed without sacrificing reliability of the algorithm.

Analysis of sketching-based randomized algorithms can often be understood in two parts. In the first part, one acquires a sketch and assumes that it retains some geometric information of interest from the data matrix, proceeding to analyze the algorithm as though it were deterministic (since no randomization is used after the sketching operator is applied). In the second part, one uses machinery from random matrix theory to analyze the probability with which the assumption about the sketch holds. The analysis we provide for CQRRPT follows this tradition. However, we focus on structural conditions which are more fine-grained than is commonly practiced in the literature. The best example of this is our treatment

---

<sup>1</sup>pronounced “see-crypt”

of a *subspace embedding*, which has been used with a great success in similar algorithmic contexts as we explain in Section 1.3. For a much broader overview of techniques in the field, we refer the reader to the recent monograph on the topic [MDM<sup>+</sup>23].

## 1.2 The CholeskyQR method and its variants

CQRRPT relies on the so-called *CholeskyQR* algorithm as one of its core computational steps. The idea behind CholeskyQR is very simple. Given the  $m \times n$  matrix  $\mathbf{M}$ , with  $m \geq n$ , if we compute the Gram matrix  $\mathbf{G} = \mathbf{M}^* \mathbf{M}$ , and if we can factor  $\mathbf{G} = \mathbf{R}^* \mathbf{R}$  for an non-singular upper-triangular matrix  $\mathbf{R}$ , then we can obtain the Q-factor with right-application of trivially invertible  $\mathbf{R}$ :  $\mathbf{Q} = \mathbf{M} \mathbf{R}^{-1}$ .

**Computational profile.** Computing  $\mathbf{G}$  and  $\mathbf{R}$  in CholeskyQR can be carried out by the BLAS function SYRK and the LAPACK function POTRF, respectively. Then in the common case,  $\mathbf{Q}$  is formed with the Level 3 BLAS function TRSM. The *flop count* for CholeskyQR using these three functions is roughly  $2mn^2 + n^3/3$  [ADO94, Page 120], which is close to the  $2mn^2 - (2/3)n^3$  flop count of Householder QR computed by LAPACK’s GEQRF function [ADO94, Page 122] as long as  $m \gg n$ .

Notably, CholeskyQR returns an explicit  $\mathbf{Q}$  factor, while GEQRF outputs an implicit representation of  $\mathbf{Q}$ . In certain numerical algorithms, the use of implicit matrix orthogonalization is not just sufficient but necessary, as it yields full  $m \times m$  orthogonal transformations. This is particularly the case, for instance, in the blockwise factorization of large matrices. Nevertheless, many common numerical methods, such as subspace projection methods, require computing the  $\mathbf{Q}$  factor explicitly. Translating an implicit factor into an explicit one using LAPACK’s ORGQR function requires additional  $2mn^2 - (2/3)n^3$  flops [ADO94, Page 122]. Consequently, given  $\mathbf{M} \in \mathbb{R}^{m \times n}$ , where  $m \gg n$ , CholeskyQR requires roughly half the flops of the traditional method of obtaining a fully explicit QR factorization.

**Limitations.** Despite its simplicity and speed, CholeskyQR is rarely used in practice. Its main shortcoming is that it fails when the numerical rank of the Gram matrix falls below  $n$ . More generally, if  $\kappa(\mathbf{M})$  denotes the condition number of  $\mathbf{M}$  and  $u$  denotes the unit roundoff in working precision, then rounding errors can cause  $\mathbf{Q}^* \mathbf{Q}$  to deviate from the identity matrix by a factor of  $\mathcal{O}(u \kappa(\mathbf{M})^2)$ . We refer to this phenomenon as *orthogonality loss*.

The orthogonality loss of CholeskyQR can be mitigated by a variety of methods.<sup>2</sup> For example, *Jacobi preconditioning* normalizes all columns of  $\mathbf{M}$  to have unit norm and is known to bring the condition number of  $\mathbf{M}$  to within a constant factor of the best-possible diagonal preconditioner [Slu69]; similar results are available for normalizing column blocks via a block-diagonal preconditioner [Dem23]. Recently, it has been suggested to use the upper-triangular factor  $\mathbf{U}$  from the LU decomposition of  $\mathbf{M}$  to precondition CholeskyQR [TOO20]. Alternatively, one can use a preconditioner obtained from CholeskyQR on a regularized version of  $\mathbf{M}$  [FKN<sup>+</sup>20]. Another approach for dealing with orthogonality loss involves re-orthogonalization (essentially running CholeskyQR twice) resulting in CholeskyQR2 algorithm [FNYY14, YNYF15]. However, this method can still fail when  $\kappa(\mathbf{M}) > u^{-\frac{1}{2}}$ . Finally, a mixed precision approach computes the Gram matrix in higher precision whereby the problematic conditioning can be better controlled [YTD15].

<sup>2</sup>Indeed, this paper adds CQRRPT to the list of orthogonality-loss mitigation methods, even though CQRRPT is concerned with pivoted rather than unpivoted QR.

### 1.3 Randomized preconditioning for CholeskyQR

The algorithm we now describe serves as the starting point of our work. Given the matrix  $\mathbf{M}$ , it sketches  $\mathbf{M}$  and then uses the triangular factor of the sketch's QR decomposition as a preconditioner in CholeskyQR. Like standard (unpreconditioned) CholeskyQR, it has a hard requirement that  $\mathbf{M}$  is full rank in exact arithmetic.

1. Compute  $\mathbf{M}^{\text{sk}} = \mathbf{S}\mathbf{M}$  using a sketching operator  $\mathbf{S} \in \mathbb{R}^{d \times m}$  with  $n \leq d \ll m$ .
2. Use your favorite stable method for QR to compute  $\mathbf{Q}^{\text{sk}}, \mathbf{R}^{\text{sk}} \leftarrow \text{qr}(\mathbf{M}^{\text{sk}})$ .
3. Form  $\mathbf{M}^{\text{pre}} \leftarrow \mathbf{M}(\mathbf{R}^{\text{sk}})^{-1}$  explicitly, with TRSM from the BLAS.
4. Run CholeskyQR:  $\mathbf{Q}, \mathbf{R}^{\text{pre}} \leftarrow \text{cholqr}(\mathbf{M}^{\text{pre}})$ .
5. Set  $\mathbf{R} \leftarrow \mathbf{R}^{\text{pre}}\mathbf{R}^{\text{sk}}$  to undo the preconditioning.

This method was first introduced [FGL21] without the context of the broader RandNLA literature; it was first studied in detail with the RandNLA literature in mind in [Bal22] and subsequently in [HSBY23]. Notably, the possibility of first computing a sketch-orthonormal Q factor  $\mathbf{M}^{\text{pre}}$ , and subsequently retrieving the  $\ell_2$ -orthonormal Q factor by a CholeskyQR of  $\mathbf{M}^{\text{pre}}$  was originally proposed elsewhere [BG22, BG21]. Furthermore, the entire concept of using  $\mathbf{R}^{\text{sk}}$  as the preconditioner traces back to the *sketch-and-precondition* paradigm in RandNLA for overdetermined least squares [RT08, AMT10, MSM14]. In this context,  $\mathbf{M}^{\text{pre}}$  is only formed implicitly and is accessed as a linear operator. If a structural condition known as the *subspace embedding property* holds between  $\mathbf{S}$  and  $\text{range}(\mathbf{M})$  [DMM06, Sar06, DMMS11, Mah11], then  $\mathbf{M}^{\text{pre}}$  is nearly-orthogonal. The near-orthogonality can then be leveraged by applying an iterative solver to the preconditioned least squares problem.

For any reasonable sketching operator,  $\mathbf{S}$ , the flop count of the randomized CholeskyQR method in the preceding five-point enumeration will be  $\mathcal{O}(mn^2)$ . Whether or not practical speedup is observed depends greatly on the sketching distribution and on the method used to compute the product  $\mathbf{S}\mathbf{M}$ . If a fast sketching operator is used with  $n \lesssim d \ll m$ , then the leading term in the resulting algorithm's flop count will be  $3mn^2$ , which is only  $mn^2$  more than the standard CholeskyQR.

### 1.4 Randomization in QR with column pivoting

There are substantial efforts reported in literature on randomized methods for QRCP of general matrices, i.e., rectangular matrices of any aspect ratio of numbers of rows and columns. These efforts originate with independent contributions by Martinsson [Mar15] as well as Duersch and Gu [DG17], with subsequent extensions by Martinsson *et al.* [MQOHvdG17] and also by Xiao, Gu, and Langou [XGL17]. While there are many variations on these methods, they share a common structure that we outline here.

As input, these methods take block size parameter  $b$  and an oversampling parameter  $s$ . They start by forming a wide  $(b+s) \times n$  sketch  $\mathbf{Y} = \mathbf{S}\mathbf{M}$ , and then proceed with a three-step iterative loop.

1. Use any QRCP method to find  $P_{\text{block}}$ , a length- $b$  vector containing column indices for the first  $b$  pivots for the wide matrix  $\mathbf{Y}$ .
2. Process the tall matrix  $\mathbf{M}[:, P_{\text{block}}]$  by QRCP or unpivoted QR.
3. Suitably update  $(\mathbf{M}, \mathbf{Y})$  and return to Step 1.

The update to  $\mathbf{M}$  at Step 3 can be handled by standard methods, such as those used in blocked unpivoted Householder QR. The update to  $\mathbf{Y}$  is more subtle. If done appropriately then the leading term in the algorithm’s flop count can be the same as that of unpivoted Householder QR [DG17].

The main limitation of these methods is that their best performance is attained with small block sizes. For example,  $b = 64$  and  $s = 10$  is used in both shared- and distributed-memory settings [MQOHvdG17, XGL17]. Much larger block sizes would be needed for the updating operations to be performed near the limit of machines’ peak performance rates. One of our motivations for developing CQRRPT has been to provide an avenue to extend earlier randomized QRCP algorithms to block sizes on the order of thousands.

## 1.5 Our contributions and outline

The basic idea of CQRRPT is simple. It starts by taking the method from Section 1.3 and replacing the call to a QR function on  $\mathbf{M}^{\text{sk}}$  with a call to a QRCP function on  $\mathbf{M}^{\text{sk}}$ . It then uses the results from this call to QRCP to provide: the pivot values, an estimate of  $\mathbf{M}$ ’s numerical rank, and the information for our preconditioner in the form of an upper-triangular matrix  $\mathbf{R}^{\text{sk}}$ . The numerical rank estimate is needed to deal with the possibility that  $\mathbf{M}$  might be rank-deficient.

CQRRPT’s discovery was reported in two independent works [Bal22] and [MDM<sup>+</sup>23]. This paper is a joint effort by the authors of these works to (1) conduct thorough a theoretical analysis of this algorithm, and (2) demonstrate experimental results of a high-performance implementation of the algorithm using RandBLAS, as part of the open-source RandLAPACK library. With this in mind, we proceed with an outline of the paper.

Section 2 starts by formally introducing CQRRPT as Algorithm 1. Our formalism emphasizes how the effect of randomness on CQRRPT’s behavior can be isolated in the choice of distribution used for the sketching operator. The core operations of CQRRPT are presented in Algorithm 2, which is analyzed purely as a deterministic algorithm. In particular, Theorem 1 establishes the correctness of CQRRPT’s output, and Theorem 2 characterizes the spectrum of the preconditioned data matrix. The remaining results in the section, Theorems 3 and 4, concern the quality of the pivots that CQRRPT returns for  $\mathbf{M}$ . These results are technical, but neither their statements nor their proofs require background in numerical analysis. Proofs for this section’s results appear in Appendix A.

Section 3 concerns CQRRPT’s numerical stability. Its main result, Theorem 9, says that CQRRPT can be implemented to provide numerical stability that is *unconditional* on the input matrix. It demonstrates that with an appropriate criterion for determining numerical rank, CQRRPT will produce a decomposition with relative error and orthogonality loss on the order of machine precision, as long as the unit roundoff satisfies  $u \leq m^{-1}F(n)^{-1}$  for some low-degree polynomial  $F(n)$ . After outlining the proof of this result we explain how numerical rank selection can be performed in practice. Appendix B states and proves a more technical version of Theorem 9 in the form of Theorem 16.

Section 4 provides empirical investigations of pivot quality. It shows how easy-to-compute metrics of pivot quality compare when running the LAPACK default function (GEQP3) versus when running CQRRPT (based on applying GEQP3 to  $\mathbf{M}^{\text{sk}}$ ). The results show the effect of *coherence* – which essentially represents a condition number for the act of sampling – on the need for more expensive or less expensive sparse sketching operators [DMIMW12].

Section 5 provides performance experiments with a RandLAPACK implementation of CQRRPT. The experiments use a machine with dual 24-core Xeon Gold 6248R CPUs, where Intel MKL and RandBLAS are the underlying linear algebra libraries. We first compare

CQRRPT with alternative methods for both unpivoted and pivoted QR factorizations. Our algorithm handily beats competing methods for large matrices, and it has the advantage of a simpler representation of  $\mathbf{Q}$ . We then investigate how CQRRPT’s performance might be improved. Runtime profiling results which show that computing QRCP of the sketch via **GEQP3** can exceed the cost of CholeskyQR several times over. This motivates an experiment where QRCP on the sketch is handled by HQRPP [MQOHvdG17] (one of the randomized algorithms for QRCP of general matrices described in Section 1.4) instead of **GEQP3**.

Concluding remarks are given in Section 6.

## 1.6 Definitions and notation

Matrices appear in boldface sans-serif capital letters. The transpose of a matrix  $\mathbf{X}$  is given by  $\mathbf{X}^*$ , its  $\ell_2$  condition number is  $\kappa(\mathbf{X})$ , and its elementwise absolute value is  $|\mathbf{X}|$ . Numerical vectors appear as boldface lowercase letters, while index vectors appear as uppercase letters. The  $k \times k$  identity matrix is denoted by  $\mathbf{I}_k$ . We extract the leading  $k$  columns of  $\mathbf{X}$  by writing  $\mathbf{X}[:, 1:k]$ , while its trailing  $n - k$  columns are extracted by writing  $\mathbf{X}[:, k + 1:n]$ . The  $(i, j)^{\text{th}}$  entry of  $\mathbf{X}$  is  $\mathbf{X}[i, j]$ . Similar conventions apply to extracting the rows of a matrix or components of a vector, and all indexing is 1-based.

In this paper, we need to speak of pivoted QR decompositions of several different matrices – often at the same time. This leads us to adopt the following conventions for the factors and other induced submatrices from these decompositions.

**Leading columns of matrices subject to QRCP.** If  $J$  is a vector with its first  $k$  entries holding column indices chosen as pivots and  $\mathbf{M}$  is a matrix that we aim to decompose via QRCP, then we abbreviate

$$\mathbf{M}_k := \mathbf{M}[:, J[1:k]].$$

Of course, we often aim to decompose a *sketch*  $\mathbf{M}^{\text{sk}}$ , and for this we use the analogous notation that  $\mathbf{M}_k^{\text{sk}} := \mathbf{M}^{\text{sk}}[:, J[1:k]]$ . Suppressing the role of  $J$  in this notation should not cause confusion, since this paper does not discuss different choices for “ $J$ ” at the same time.

**Valid decompositions.** We refer to the orthogonal and triangular factors from pivoted QR decompositions by the names *Q-factors* and *R-factors*. The first  $k$  columns of a Q-factor “ $\mathbf{Q}$ ” are denoted by  $\mathbf{Q}_k$ , and the first  $k$  rows of an R-factor “ $\mathbf{R}$ ” are denoted by  $\mathbf{R}_k$ . We impose minimal requirements on these factors. To be concrete, suppose we seek a pivoted QR decomposition of a rank- $k$  matrix  $\mathbf{X}$  that has  $n$  columns. We say that  $(\mathbf{Q}, \mathbf{R}, J)$  are valid for this purpose if  $\mathbf{Q}$  is column-orthonormal,  $\mathbf{R}$  is upper-triangular, and

$$\mathbf{X}_n = \mathbf{Q}\mathbf{R} = \mathbf{Q}_k\mathbf{R}_k,$$

where  $\mathbf{X}_n = \mathbf{X}[:, J]$ . Note that this allows for R-factors that are not square.

**Partitions of R-factors.** Consider any positive integer  $k \leq n$ . For a  $k \times n$  triangular matrix  $\mathbf{R}$  and a parameter  $\ell \leq k$ , we label the individual submatrices

$$\begin{aligned} \mathbf{A}_\ell &= \mathbf{R}[1:\ell, 1:\ell], \\ \mathbf{B}_\ell &= \mathbf{R}[1:\ell, \ell + 1:n], \text{ and} \\ \mathbf{C}_\ell &= \mathbf{R}[\ell + 1:k, \ell + 1:n], \end{aligned}$$

so as to cleanly write

$$\mathbf{R} = \begin{bmatrix} \mathbf{A}_\ell & \mathbf{B}_\ell \\ & \mathbf{C}_\ell \end{bmatrix}.$$

We apply similar naming conventions to triangular matrices in other contexts. For example, we write  $\mathbf{A}_p^{\text{sk}}$  in reference to the leading  $p \times p$  submatrix of a  $k \times n$  triangular matrix  $\mathbf{R}^{\text{sk}}$  (defined when  $p \leq k \leq n$ ).

## 2 Getting to know our algorithm

The pseudocode below (Algorithm 1) introduces the CQRRPT algorithm. This algorithm’s speed and reliability are affected decisively by the distribution from which  $\mathbf{S}$  is sampled, and it has two parameters that control this distribution. The higher-level parameter, denoted by  $\mathcal{F}$ , is a *distribution family*. This is an association of matrix dimensions  $(d, m)$  to probability distributions over matrices with those dimensions; the distribution in  $\mathcal{F}$  over  $d \times m$  matrices is denoted by  $\mathcal{F}_{d,m}$ . The lower-level parameter is a *sampling factor*, which controls the size (number of rows, denoted “ $d$ ”) of the sketch relative to the number of columns in  $\mathbf{M}$ .

---

### Algorithm 1 CholeskyQR with randomization and pivoting for tall matrices

---

**Required inputs.** An  $m \times n$  matrix  $\mathbf{M}$ .

**Optional inputs.** A scalar  $\gamma$  that sets the size of the sketch relative to  $n$  ( $\gamma \geq 1$ ).  
A specification for a distribution family  $\mathcal{F}$ .

**Outputs.** Orthogonal  $\mathbf{Q} \in \mathbb{R}^{m \times k}$ , upper-triangular  $\mathbf{R} \in \mathbb{R}^{k \times n}$ , and a permutation vector  $J$  of length  $n$ . (We have  $k \leq \text{rank}(\mathbf{M})$ , where equality holds generically.)

- 1: **function** `cqrrpt`( $\mathbf{M}, \gamma, \mathcal{F}$ )
  - 2:   If  $\mathcal{F}$  is not provided, set it to a default family of sparse sketching distributions.
  - 3:   If  $\gamma$  is not provided, set  $\gamma = 1.25$ .
  - 4:   Set  $d = \lceil \gamma n \rceil$ .
  - 5:   Randomly sample a sketching operator  $\mathbf{S}$  from  $\mathcal{F}_{d,m}$ .
  - 6:   **return** `cqrrpt_core`( $\mathbf{M}, \mathbf{S}$ ).
- 

The actual work in CQRRPT is contained in a deterministic function called `cqrrpt_core` (Algorithm 2). We introduce this function and describe its behavior in exact arithmetic over the course of Sections 2.1 and 2.2. Our descriptions prominently feature the concept of *restricted singular values*. In our context, the restricted singular values for  $\mathbf{S}$  on a subspace  $L$  are the singular values of any matrix of the form  $\mathbf{S}\mathbf{U}$ , where the columns of  $\mathbf{U}$  give an orthonormal basis for  $L$ . The *restricted condition number* of  $\mathbf{S}$  on  $L$  is simply the ratio of its largest to smallest restricted singular values. We address how choices of distribution families affect CQRRPT’s probabilistic behavior in Section 2.3. This also includes an explanation of how standard results from random matrix theory can be used to bound the restricted singular values of  $\mathbf{S}$  on  $\text{range}(\mathbf{M})$ , in a way that depends on  $\mathcal{F}$  and  $\gamma$  but *not* on  $\mathbf{M}$ .

### 2.1 Algorithm 2 : `cqrrpt_core`

In what follows we use a black-box function called `qrqp`. This can refer to any algorithm that is guaranteed to produce a decomposition that is “valid,” in the sense of Section 1.6.

---

**Algorithm 2 : crrpt\_core**


---

**Input:** A matrix  $\mathbf{M} \in \mathbb{R}^{m \times n}$ , and a sketching operator  $\mathbf{S} \in \mathbb{R}^{d \times m}$  where  $n \leq d \ll m$ .

- 1: **function** crrpt\_core( $\mathbf{M}, \mathbf{S}$ )
- 2:   Sketch  $\mathbf{M}^{\text{sk}} = \mathbf{S}\mathbf{M}$
- 3:   Decompose  $[\mathbf{Q}^{\text{sk}}, \mathbf{R}^{\text{sk}}, J] = \text{qrqp}(\mathbf{M}^{\text{sk}})$
- 4:   Determine  $k = \text{rank}(\mathbf{R}^{\text{sk}})$   
       // ^ see page 9 for discussion on determining numerical rank
- 5:   Truncate and precondition  $\mathbf{M}^{\text{pre}} = \mathbf{M}_k(\mathbf{A}_k^{\text{sk}})^{-1}$   
       // ^ recall our notation that  $\mathbf{M}_k := \mathbf{M}[:, J[1:k]]$  and  $\mathbf{A}_k^{\text{sk}} := \mathbf{R}^{\text{sk}}[1:k, 1:k]$
- 6:   Decompose  $[\mathbf{Q}_k, \mathbf{R}^{\text{pre}}] = \text{cholqr}(\mathbf{M}^{\text{pre}})$   
       // ^  $\mathbf{Q}_k$  is  $m \times k$  and  $\mathbf{R}^{\text{pre}}$  is  $k \times k$
- 7:   Undo preconditioning  $\mathbf{R}_k = \mathbf{R}^{\text{pre}}\mathbf{R}_k^{\text{sk}}$   
       // ^ recall our notation that  $\mathbf{R}_k^{\text{sk}} := \mathbf{R}^{\text{sk}}[1:k, :]$ .
- 8:   **return**  $\mathbf{Q}_k, \mathbf{R}_k, J$

---

**Correctness.** There are two pressing questions for Algorithm 2.

1. Under what conditions does it actually obtain a decomposition of  $\mathbf{M}$ ?
2. Just how “safe” is its use of CholeskyQR on Line 6?

Section 3 gives highly technical answers to these questions in finite-precision arithmetic. Here are simpler answers under the assumption of computation in exact arithmetic.

**Theorem 1.** *If the restricted condition number of  $\mathbf{S}$  on the range of  $\mathbf{M}$  is finite, then crrpt\_core( $\mathbf{M}, \mathbf{S}$ ) returns a valid column-pivoted QR decomposition of  $\mathbf{M}$ .*

**Theorem 2.** *Let  $\mathbf{M}^{\text{pre}}$  be as on Line 5 of Algorithm 2 for inputs  $\mathbf{M}$  and  $\mathbf{S}$ . The singular values of  $\mathbf{M}^{\text{pre}}$  are the inverses of the restricted singular values of  $\mathbf{S}$  on  $\text{range}(\mathbf{M})$  – provided all of the latter quantities are nonzero.*

Theorem 1 is a correctness result for Algorithm 2. It suggests CRRPT is worth studying, but it makes no predictions for CRRPT’s numerical behavior. Theorem 2 *does* make a prediction about CRRPT’s numerical behavior, in the sense that rounding errors in its CholeskyQR step should have no direct dependence on the spectrum of  $\mathbf{M}$ . It also implies that probabilistic bounds on restricted singular values from random matrix theory translate to probabilistic bounds on the condition number of the matrix that we process by CholeskyQR. Proofs of these results are deferred to Appendix A.1.

**Arithmetic complexity.** The arithmetic complexity of Algorithm 2 depends on how we compute and then decompose  $\mathbf{M}^{\text{sk}}$ . Since there are many practical ways to handle the first of these operations, we shall simply say its cost in flops is  $C_{\text{sk}}$ . There are also many ways one might perform the second operation, but the most practical is to use the LAPACK function GEQP3. With this choice, the algorithm’s flop count is

$$2mk^2 + mk(k+1) + 4dnk - 2k^2(d+n) + 5k^3/3 + C_{\text{sk}} \quad (1)$$

plus lower-order terms. This implies that CRRPT’s asymptotic flop count has the leading term  $3mn^2$  for a full-rank data matrix. (See Appendix A.2 for a derivation of (1).) Furthermore, in certain applications, it may suffice to operate with the  $m \times k$  Q-factor in implicit



form. In such cases, CQRRPT can provide  $\mathbf{Q}$  as a composition of two matrices,  $\mathbf{M}^{\text{pre}}$  and  $(\mathbf{R}^{\text{pre}})^{-1}$ , without sacrificing numerical stability (as is clear from our stability analysis). This can decrease the leading term in the arithmetic complexity to  $2mn^2$ .

It is concluded that with a suitable sketching matrix, the flop count in CQRRPT for obtaining a QR factorization with implicit  $m \times k$  Q-factor is asymptotically the same as that of unpivoted Householder QR. Furthermore, acquiring an explicit representation of the Q-factor from Householder QR requires using LAPACK function `ORGQR` and increases the leading-order term in the flop count by another  $2mn^2$  [ADO94]. This implies that in applications that necessitate performing an explicit orthogonalization, CQRRPT can be up to  $\frac{4}{3} \times$  cheaper in terms of flops than unpivoted Householder QR.

**Communication cost.** CQRRPT lends itself naturally to distributed computation. Here it is prudent to choose the sketching distribution that allows for a blockwise implementation of  $\mathbf{S} \cdot \mathbf{M}$  with quasi-optimal communication cost and permits the smallest possible value of  $d$  while retaining good statistical properties. In both theory and practice, this can be achieved through the use of Gaussian sketching operators (see Section 2.3.2) with  $d = 1.25n$ .

Consider a popular setting where  $\mathbf{M}$  is distributed block row-wise across  $p \leq m/d$  processors, each of which has at least  $2dn + n^2$  words of available memory. Here it is straightforward to attain near-optimal communication cost for performing the matrix multiplications  $\mathbf{S} \cdot \mathbf{M}$  and  $(\mathbf{M}^{\text{pre}})^* \cdot (\mathbf{M}^{\text{pre}})$  [DGHL12]. To be explicit, the computation of  $\mathbf{S} \cdot \mathbf{M}$  proceeds with local multiplications of blocks of  $\mathbf{M}$  with the corresponding blocks of columns of  $\mathbf{S}$  (using  $dn$  words of memory) and summing the contributions using an all-reduce operation (using another  $dn$  words of memory). From there, each processor performs QRCP on  $\mathbf{M}^{\text{sk}}$ , recovers  $\mathbf{A}_k^{\text{sk}}$  from  $\mathbf{R}^{\text{sk}}$ , and applies its inverse to the corresponding local block of  $\mathbf{M}$ . When using the classical binomial tree version of all-reduce, the overall computation of the preconditioned matrix  $\mathbf{M}^{\text{pre}}$  requires one global synchronization,  $2 \log_2 p$  messages,  $2dn \log_2 p$  communication volume, and two data passes. Adding the cost of the CholeskyQR step [ND15], we get the total cost of CQRRPT: two global synchronizations,  $4 \log_2 p$  messages,  $(2dn + n^2) \log_2 p$  communication volume, and three data passes. Notably, if we used the recursive-halving version of all-reduce [TRG05], the communication volume can be improved to a mere  $2dn + n^2$ .

In general computational environments and data layouts, using an unstructured sketching operator with  $d \approx n$  should incur a similar cost in terms of synchronization, inter-processor communication, and memory footprint as computing the Gram matrix  $\mathbf{M}^* \mathbf{M}$  in CholeskyQR. This implies that CQRRPT can achieve comparable efficiency in terms of modern efficiency metrics as CholeskyQR2 while providing greater stability. In particular, CQRRPT stands to inherit the computational advantages of CholeskyQR2 on massively parallel architectures [FNYY14].

**Determining numerical rank.** When CQRRPT computes  $k = \text{rank}(\mathbf{R}^{\text{sk}})$  for the upper-triangular matrix  $\mathbf{R}^{\text{sk}}$ , the assumption of exact arithmetic implies that one can simply count the number of rows in  $\mathbf{R}^{\text{sk}}$  that are nonzero. In practice, deciding on a proper way of estimating numerical rank  $k$  is both important and nuanced. The method that we use in our implementation of CQRRPT has two stages and only entails  $\mathcal{O}(n)$  work; this method is described in Section 3 along with our numerical analysis results.

## 2.2 How Algorithm 2 inherits rank-revealing properties

Here we explain how CQRRPT inherits pivot quality properties from its underlying `qrqp` function. To describe these properties, we speak in terms of a matrix  $\mathbf{X}$  consisting of  $n$

columns and at least as many rows,<sup>3</sup> along with its decomposition  $[\mathbf{Q}, \mathbf{R}, \mathbf{J}] = \text{qrqp}(\mathbf{X})$ . For an index  $\ell \leq k = \text{rank}(\mathbf{X})$ , we use  $(\mathbf{A}_\ell, \mathbf{B}_\ell, \mathbf{C}_\ell)$  to denote submatrices of  $\mathbf{R}$  following the conventions established in Section 1.6.

Our first property of interest, *rank revealing QR* (RRQR), concerns how well the spectrum of  $\mathbf{A}_\ell$  approximates the leading singular values of  $\mathbf{X}$ , and how well the spectrum of  $\mathbf{C}_\ell$  approximates the trailing singular values of  $\mathbf{X}$ . When  $\mathbf{X}$  is fixed, we can describe the approximation quality by a sequence of constants  $f_1, \dots, f_k$ , all at least unity. Formally,  $\text{qrqp}$  satisfies the RRQR property for  $\mathbf{X}$  up to a factors  $(f_\ell)_{\ell=1}^k$  if, for all  $\ell \leq k$ , we have

$$\sigma_j(\mathbf{A}_\ell) \geq \frac{\sigma_j(\mathbf{X})}{f_\ell} \quad \text{for all } j \leq \ell, \quad (2a)$$

and

$$\sigma_j(\mathbf{C}_\ell) \leq f_\ell \sigma_{\ell+j}(\mathbf{X}) \quad \text{for all } j \leq k - \ell. \quad (2b)$$

**Theorem 3.** *Suppose  $\text{qrqp}$  satisfies the RRQR property for  $\mathbf{SM}$  up to factors  $(f_\ell)_{\ell=1}^k$ . If  $\kappa$  denotes the restricted condition number of  $\mathbf{S}$  on  $\text{range}(\mathbf{M})$ , then  $\text{cqrqp\_core}(\cdot, \mathbf{S})$  satisfies the RRQR property for  $\mathbf{M}$  up to factors  $(\kappa f_\ell)_{\ell=1}^k$ .*

It is common to ask for RRQR factors of a QRCP algorithm that do not depend on the numerical properties of the matrix to be decomposed. That is, it is common to ask that a QRCP algorithm be associated with a *function*  $f$ , where the evaluations  $(f(\ell, n))_{\ell=1}^k$  provide RRQR factors for any rank- $k$  matrix with  $n$  columns on which the algorithm might be applied. This is a significant requirement. QRCP with the max-norm pivot rule does not satisfy the resulting requirements for *any* function  $f$ , as can be seen by taking a limit of Kahan matrices of fixed dimension [GE96, Example 1]. Still, there are several QRCP algorithms that can ensure the RRQR property, where  $f(\ell, n)$  is a function that is not only independent of  $\mathbf{M}$  but also bounded by a low-degree polynomial in  $\ell$  and  $n$ . Theorem 3 shows that if CQRPT is configured to use such an algorithm, then it will satisfy a nearly identical RRQR property.

Next, we consider the *strong RRQR* property, which concerns our ability to use  $\mathbf{R}$  to find a well-conditioned basis for an approximate null space of  $\mathbf{X}_n$ . The particular basis is the columns of the block matrix  $\mathbf{Y} = [\mathbf{A}_\ell^{-1} \mathbf{B}_\ell; -\mathbf{I}]$ , which satisfies  $\|\mathbf{X}_n \mathbf{Y}\| = \|\mathbf{C}_\ell\|$  in every unitarily invariant norm. For our purposes, we say that  $\text{qrqp}$  satisfies the strong RRQR property for  $\mathbf{X}$  with factors  $(f_\ell)_{\ell=1}^k$  and  $(g_\ell)_{\ell=1}^k$  when the former factors satisfy (2a)-(2b) and the latter factors satisfy

$$\|\mathbf{A}_\ell^{-1} \mathbf{B}_\ell\|_2 \leq g_\ell \quad (3)$$

for all  $\ell \leq k$ .

**Theorem 4.** *Suppose  $\text{qrqp}$  satisfies the strong RRQR property for  $\mathbf{SM}$  with factors  $(f_\ell)_{\ell=1}^k$  and  $(g_\ell)_{\ell=1}^k$ . If  $\kappa$  is the restricted condition number of  $\mathbf{S}$  on  $\text{range}(\mathbf{M})$ , then  $\text{cqrqp\_core}(\cdot, \mathbf{S})$  satisfies the strong RRQR properties for  $\mathbf{M}$  up to factors  $(\kappa f_\ell)_{\ell=1}^k$  and  $(g_\ell + \kappa f_\ell^2)_{\ell=1}^k$ .*

As with RRQR, we can ask that a QRCP algorithm be associated with *functions*  $f$  and  $g$  for which  $(f(\ell, n))_{\ell=1}^k$  and  $(g(\ell, n))_{\ell=1}^k$  provide strong RRQR factors for any rank- $k$  matrix with  $n$  columns on which the algorithm might be applied. The first algorithm that could ensure this was introduced by Gu and Eisenstat [GE96]. Setting the tuning parameter of their algorithm to two leads to strong RRQR factors

$$f(\ell, n) = \sqrt{1 + 4\ell(n - \ell)} \quad \text{and} \quad g(\ell, n) = 2\sqrt{\ell},$$

---

<sup>3</sup>Which we might take as  $\mathbf{X} = \mathbf{M}$  or  $\mathbf{X} = \mathbf{M}^{\text{sk}}$ , depending on context.

with a runtime of  $\mathcal{O}(mn^2)$  for an  $m \times n$  matrix with  $m \geq n$ . Theorem 4 shows that if CQRRPT uses this algorithm for QRCF on  $\mathbf{S}\mathbf{M}$ , then it will enjoy an analogous strong RRQR property with some increase to  $g$ .

## 2.3 Probabilistic aspects of CQRRPT

Because CQRRPT randomly samples  $\mathbf{S}$  from a probability distribution, any quantity that  $\mathbf{S}$  affects in Algorithm 2 can be regarded as a random variable. Most notably, this includes  $\mathbf{M}^{\text{pre}}$  (the matrix that CQRRPT passes to CholeskyQR) and the condition number of  $\mathbf{M}^{\text{pre}}$ . CQRRPT’s numerical behavior is closely related to the distribution of this latter random variable. In particular, if we are to understand its behavior, it is important to explore the following question.

How can we bound the probability that  $\kappa(\mathbf{M}^{\text{pre}})$  stays within some prescribed limit, *no matter the matrix  $\mathbf{M}$* ?

The answer to this question depends greatly on the distribution family  $\mathcal{F}$  and the sampling factor  $\gamma$  provided to CQRRPT. Here, we provide a range of answers based on different choices for these parameters. We also make recommendations for choosing these parameters in practice, to balance competing needs for algorithm speed and reliability.

### 2.3.1 Sketching distribution families: examples and intuition

For a fixed distribution family  $\mathcal{F}$ , recall that we use “ $\mathcal{F}_{d,m}$ ” for the distribution in  $\mathcal{F}$  over  $d \times m$  matrices. Below we describe the structure of random matrices  $\mathbf{S}$  drawn from such distributions in various families when  $d \ll m$ .

- *Gaussian matrices.* The entries of  $\mathbf{S}$  are iid Gaussian random variables with mean zero and variance  $1/\sqrt{d}$ .
- *SASOs* (short-axis-sparse operators). The columns of  $\mathbf{S}$  are independent. Each column has a fixed number of nonzeros, and the nonzero values are chosen to be  $\pm 1/\sqrt{d}$  with equal probability.<sup>4</sup> The precise number of nonzeros in each column,  $\ell$ , is a tuning parameter that can be changed to define different families  $\mathcal{F}$ . In practice, it is common to keep  $\ell$  between one and eight, even when  $d$  is on the order of tens of thousands.
- *SRFTs* (subsampled randomized fast trigonometric transforms). A fast trigonometric transform is an orthogonal or unitary transformation such as the DFT, the DCT, or the Walsh-Hadamard transform.<sup>5</sup> An SRFT is a composition of three operators:  $\mathbf{S} = \sqrt{m/d}\mathbf{C}\mathbf{F}\mathbf{D}$ , where  $\mathbf{D}$  is a diagonal matrix with diagonal populated by Rademacher random variables (if  $\mathbf{S}$  is real) or Steinhaus random variables (otherwise),  $\mathbf{F}$  is a fast trigonometric transform, and  $\mathbf{C}$  is obtained by randomly permuting the columns of  $[\mathbf{I}_d, \mathbf{0}_{d \times (m-d)}]$ .

These families share key properties. First, if  $\mathbf{S}$  is a random matrix sampled from  $\mathcal{F}_{d,m}$ , then its expected covariance matrix satisfies  $\mathbb{E}[\mathbf{S}^*\mathbf{S}] = \mathbf{I}_m$ . Second, if  $\mathbf{U}$  is an  $m \times k$  column-orthonormal matrix and  $d$  is sufficiently large relative to  $k$ , then the sketched Gram matrix  $\mathbf{U}^*\mathbf{S}^*\mathbf{S}\mathbf{U}$  concentrates strongly around  $\mathbb{E}[\mathbf{U}^*\mathbf{S}^*\mathbf{S}\mathbf{U}] = \mathbf{I}_k$ . To rephrase this second property:  $\mathbf{S}\mathbf{U}$  should concentrate strongly around the manifold  $M_{d,k}$  of  $d \times k$  column-orthonormal matrices.

<sup>4</sup>For the etymology of these sketching operators, see [MDM+23].

<sup>5</sup>These are used for complex matrices, real matrices, and matrices where  $m$  is a power of two, respectively.

One can see the usefulness of these properties in our context by considering Theorem 2. Specifically, if  $\text{range}(\mathbf{U}) = \text{range}(\mathbf{M})$  and  $\mathbf{SU}$  has rank- $k$ , then the singular values of  $\mathbf{M}^{\text{pre}}$  will equal those of  $(\mathbf{SU})^\dagger$ . Therefore the desirable phenomenon of  $\mathbf{M}^{\text{pre}}$  concentrating around  $M_{m,k}$  is equivalent to  $\mathbf{SU}$  concentrating around  $M_{d,k}$ .

### 2.3.2 Oblivious subspace embeddings

Let  $\mathbf{U}$  be a matrix whose columns are an orthonormal basis for a linear subspace  $L \subset \mathbb{R}^m$ , and let  $\mathbf{S}$  be a sketching operator on  $L$ . In the context of RandNLA, here is the most common way to quantify the interaction between  $\mathbf{S}$  and  $L$ .

**Definition 5.** We call  $\mathbf{S}$  a subspace embedding for  $L$  with distortion  $\delta \in [0, 1]$  if

$$1 - \delta \leq \sigma_{\min}(\mathbf{SU}) \quad \text{and} \quad \sigma_{\max}(\mathbf{SU}) \leq 1 + \delta. \quad (4)$$

Such an operator is also called a  $\delta$ -embedding for  $L$ .

Subspace embeddings were first introduced for the least squares problem [DMM06] and were first used in data-oblivious form by [Sar06, DMMS11]. They were popularized in data-oblivious form by [Woo14], and they have been used to construct preconditioners for iterative algorithms for the least squares problem [RT08, AMT10, MSM14].

There is theory available on how to choose  $d$  so that a sample from  $\mathcal{F}_{d,m}$  will be a  $\delta$ -embedding for any fixed  $n$ -dimensional linear subspace with high probability. We can rely on this theory to select  $d$  in practice for very well-behaved distribution families. For example, here is the now-standard result for Gaussians, where  $L$  is an  $n$ -dimensional subspace in  $\mathbb{R}^m$ .

**Theorem 6** (See [MT20], §8 ). *Fix any  $t > 0$  such that  $\delta = ((\sqrt{n} + 1)/\sqrt{d} + t) < 1$ . If  $\mathbf{S}$  is a  $d \times m$  Gaussian operator, then it will be a  $\delta$ -embedding for  $L$  with probability at least  $1 - 2\exp(-dt^2/2)$ .*

Results for the more sophisticated families (SASOs or SRFTs) — which are often of interest since they are algorithmically more attractive than Gaussian matrices — tend to be pessimistic compared to what is observed in practice. Still, we give representative results for these families below.

**Theorem 7** ([Coh16], Theorem 4.2). *Fix any  $B > 2$ ,  $t \geq 1$ , and  $\delta < 1/2$ . There are absolute constants  $c_1, c_2$  where, upon taking*

$$d \geq c_1 t (B \log B) (n \log n) / \delta^2 \quad \text{and} \quad s \geq c_2 t (\log B) (\log n) / \delta,$$

*sampling a  $d \times m$  SASO with  $s$  nonzeros per column provides a  $\delta$ -embedding for  $L$  with probability at least  $1 - B^{-t}$ .*

**Theorem 8** ([Tro11], Theorem 1.3). *If  $\mathbf{S}$  is a  $d \times m$  SRFT based on the Walsh-Hadamard Transform with*

$$4 \left( \sqrt{n} + \sqrt{8 \log(nm)} \right)^2 \log n \leq d \leq m,$$

*then it will be a 0.6-embedding for  $L$  with probability at least  $1 - \mathcal{O}(n^{-1})$ .*

### 3 Numerical stability

This section analyzes `cqrrpt_core` (Algorithm 2) under the assumption that all algebraic operations in it and in its subroutines are performed in finite precision arithmetic. Suppose for concreteness that we have

$$[\mathbf{Q}_k, \mathbf{R}_k, J] = \text{cqrrpt\_core}(\mathbf{M}, \mathbf{S}), \quad (5)$$

where  $\mathbf{Q}_k$  is  $m \times k$  and  $\mathbf{R}_k$  is  $k \times n$  and upper-triangular. In these terms, our analysis is concerned with bounding the *reconstruction error*  $\|\mathbf{M}_n - \mathbf{Q}_k \mathbf{R}_k\|_F / \|\mathbf{M}\|_F$  and the *orthogonality loss*  $\|\mathbf{Q}_k^* \mathbf{Q}_k - \mathbf{I}_k\|_2$ .

Proving bounds on these quantities requires assumptions on the `qrqp` and `rank` subroutines. So far we have said very little about these points because they are ultimately design questions that have no single answer. In this section, our goal is to show that CQRRPT can be numerically stable *unconditionally* on the input matrix and with mild assumptions on the implementation of its underlying linear algebraic operations. That is, we want to show that `qrqp` and `rank` can be efficiently implemented so reconstruction error and orthogonality loss are bounded above by a low-degree polynomial in  $(n, m)$ , independent of the numerical properties of  $\mathbf{M}$ . Such a result will directly imply that CQRRPT's properties introduced in Section 2 and proven in Appendix A are preserved under finite precision arithmetic.

**New notation.** Up until now the  $m \times k$  and  $k \times k$  matrices  $\mathbf{M}^{\text{pre}}$  and  $\mathbf{R}^{\text{pre}}$  have been referred to without notational dependence on  $k$ . Our upcoming discussions would be impaired if we continued to use this notation. Therefore, moving forward, we use  $\mathbf{M}_k^{\text{pre}}$  and  $\mathbf{R}_k^{\text{pre}}$  for these matrices. We can select submatrices from them using notation consistent with Section 1.6. For example, we can speak of a parameter  $\ell < k$  and use  $\mathbf{M}_\ell^{\text{pre}}$  in reference to the first  $\ell$  columns of  $\mathbf{M}_k^{\text{pre}}$ . Similarly, we can use  $\mathbf{A}_\ell^{\text{pre}}$  to denote the leading  $\ell \times \ell$  submatrix of  $\mathbf{R}_k^{\text{pre}}$ .

Additionally, we adopt the notation where scalars  $x$  and  $y$  are said to satisfy  $x \lesssim y$  if  $x \leq cy + G(n)u$ , where  $c$  is a constant close to 1,  $G(n)$  is a low-degree polynomial, and  $u$  is a unit roundoff. Moreover, we use  $\|\cdot\|$  to denote either the Frobenius or the spectral norm.

#### 3.1 Summary

##### 3.1.1 The challenge

One of our goals in CQRRPT's numerical analysis is essentially to specify how the `rank` function on Line 4 of `cqrrpt_core` should be implemented. Therefore one should consider  $k$  as something that we *choose*, rather than something that takes a specific fixed value.

With that established, let us outline how  $k$  affects reconstruction error and orthogonality loss. In the time-honored tradition of adding zero and applying the triangle inequality, one can obtain the following bound on reconstruction error committed in the preconditioning step:

$$\|\mathbf{M}_n - \mathbf{M}^{\text{pre}} \mathbf{R}_k^{\text{sk}}\| \leq \underbrace{\|\mathbf{M}_n - \mathbf{M}_k (\mathbf{A}_k^{\text{sk}})^{-1} \mathbf{R}_k^{\text{sk}}\|}_{\text{truncation error}} + \|(\mathbf{M}_k - \mathbf{M}^{\text{pre}} \mathbf{A}_k^{\text{sk}}) (\mathbf{A}_k^{\text{sk}})^{-1} \mathbf{R}_k^{\text{sk}}\|. \quad (6)$$

We have labeled the more opaque term in (6) the *truncation error*. To better understand it, suppose  $\delta$  is the distortion of  $\mathbf{S}$  for the range of  $\mathbf{M}$ . We claim that under mild assumptions for the accuracy of operations on Lines 2 and 3, and an assumption that  $\mathbf{A}_k^{\text{sk}}$  is not too ill-conditioned, one can bound

$$\|\mathbf{M}_n - \mathbf{M}_k (\mathbf{A}_k^{\text{sk}})^{-1} \mathbf{R}_k^{\text{sk}}\| / \|\mathbf{M}\| \lesssim (1 + \delta) \|\mathbf{C}_k^{\text{sk}}\| / \|\mathbf{M}^{\text{sk}}\|. \quad (7)$$

Since  $\|\mathbf{C}_k^{\text{sk}}\|$  is decreasing with  $k$ , this bound suggests that  $k$  should be large to keep reconstruction error under control.

Unfortunately, if  $\mathbf{M}$  is ill-conditioned, then choosing  $k$  too large can pose severe problems. The basic reason for this stems from the fact that  $\kappa(\mathbf{A}_n^{\text{sk}})$  can be as large as  $\kappa(\mathbf{SM})$ , which in turn can be as large as  $\frac{1+\delta}{1-\delta} \kappa(\mathbf{M})$ . This suggests that  $\mathbf{A}_k^{\text{sk}}$  can be ill-conditioned when  $k$  is large, even when  $\delta$  is small. This matters since larger condition numbers for  $\mathbf{A}_k^{\text{sk}}$  risk larger rounding errors at the step when we form the  $m \times k$  matrix  $\mathbf{M}^{\text{pre}}$ . If this step is performed inaccurately, then  $\kappa(\mathbf{M}^{\text{pre}})$  might be far from one even if  $\delta$  is small, which risks orthogonality loss in  $\mathbf{Q}_k$  that cannot be controlled by our choice of sketching distribution for Algorithm 1.

### 3.1.2 A high-level result

The tension described above raises an important question. Can we be certain that there *exists* a truncation index  $k$  so that both reconstruction error and orthogonality loss are kept near machine precision? The following result says the answer is yes, provided the QRCP of  $\mathbf{M}^{\text{sk}}$  is (sufficiently) strongly rank-revealing.

**Theorem 9** (Simplified version of Theorem 16 from Appendix B). *Consider Algorithm 2 where Line 5 is executed with unit roundoff  $\mathbf{u}$ , and other lines are executed with unit roundoff  $\tilde{\mathbf{u}}$ . Assume that the qrqp subroutine at Line 3 produces  $\mathbf{Q}^{\text{sk}}$  and  $\mathbf{R}^{\text{sk}}$  by a pivoted Householder QR process or pivoted Givens QR process, and that its pivots satisfy the strong rank-revealing property for  $(\mathbf{Q}^{\text{sk}}, \mathbf{R}^{\text{sk}}, \mathbf{M}^{\text{sk}})$  with factors  $f_\ell, g_\ell \leq 2\sqrt{n\ell}$ . In addition, suppose  $\mathbf{S}$  is a  $\delta$ -embedding for  $\text{range}(\mathbf{M})$  with  $\delta \leq \frac{1}{4}$ .*

*There exists a truncation index  $k$  and low-degree polynomials  $G_1, \dots, G_5$  such that if  $\tilde{\mathbf{u}} \leq m^{-1}G_1(n)^{-1}\mathbf{u}$  and  $\mathbf{u} \leq G_2(n)^{-1}$ , then*

$$\|\mathbf{M}_n - \mathbf{M}^{\text{pre}} \mathbf{R}_k^{\text{sk}}\| \leq G_3(n)\mathbf{u} \|\mathbf{M}\| \quad \text{and} \quad \kappa(\mathbf{M}^{\text{pre}}) \leq 1.8. \quad (8)$$

Furthermore, as a direct consequence of Eq. (8), we have

$$\|\mathbf{M}_n - \mathbf{Q}_k \mathbf{R}_k\| \leq G_4(n)\mathbf{u} \|\mathbf{M}\| \quad \text{and} \quad \|\mathbf{Q}_k^* \mathbf{Q}_k - \mathbf{I}\| \leq G_5(n)\mathbf{u}. \quad (9)$$

We have chosen a computational model with two unit roundoffs to highlight an important property of the preconditioner – the ability to maintain numerical stability with a larger unit roundoff at the dominant Line 5, independent of  $m$ . This property may have significant implications for multi- and low-precision arithmetic architectures. Clearly, the result can also be used in the computational model with a single roundoff.

We note that Theorem 9 is an *existential* result for a suitable truncation rank  $k$ . Our proof of this result includes a method for how such  $k$  can be identified efficiently, under the stated assumptions on the unit roundoffs. However, in practice, the unit roundoff is usually a constant that does not change with the matrix dimensions. This creates a need for a separate and more practical way to choose the truncation rank, which is a topic we address in Section 3.3.

## 3.2 Proof sketch for Theorem 9

The following lemma shows that Eq. (9) in Theorem 9 directly follows from Eq. (8).

**Lemma 10.** Consider Lines 5 to 7 of Algorithm 2 where the computations are performed with unit roundoff  $\tilde{u} \leq 0.00022m^{-1}n^{-1}$ .

$$\text{If} \quad \|\mathbf{M}_n - \mathbf{M}_k^{\text{pre}} \mathbf{R}_k^{\text{sk}}\|_2 \leq 0.01 \|\mathbf{M}\|_2 \text{ and } \kappa(\mathbf{M}_k^{\text{pre}}) \leq 6, \quad (10)$$

$$\text{then} \quad \|\mathbf{M}_n - \mathbf{Q}_k \mathbf{R}_k\|_F \leq \|\mathbf{M}_n - \mathbf{M}_k^{\text{pre}} \mathbf{R}_k^{\text{sk}}\|_F + 60n^2 \tilde{u} \|\mathbf{M}\|_2, \quad (11)$$

$$\text{and} \quad \|\mathbf{Q}_k^* \mathbf{Q}_k - \mathbf{I}\|_2 \leq 180mn\tilde{u}. \quad (12)$$

We prove Lemma 10 in Appendix B.1 by straightforward methods. Taking it as given, the question is how to choose  $k$  so the property (8) in Theorem 9 holds. We call this the *preconditioner stability question*. In brief, the main idea is to choose  $k$  so that

$$\|\mathbf{C}_k^{\text{sk}}\|/\|\mathbf{R}^{\text{sk}}\| \leq G_0(n)\mathbf{u} \leq \|\mathbf{C}_{k-1}^{\text{sk}}\|/\|\mathbf{R}^{\text{sk}}\|, \quad (13)$$

for some suitable low-degree polynomial  $G_0(n)$ . Our formal specification for how to choose  $k$  is given in the highly technical Theorem 16, which is stated and proven in Appendix B. In what follows, we outline the key steps in the argument for proving that theorem, using the same notation as in our formal proofs.

**Truncation ensures full numerical rank.** Choosing  $k$  to satisfy (13) ensures that  $\mathbf{A}_k^{\text{sk}}$  is numerically full-rank. Assuming the stated RRQR properties of  $\mathbf{R}^{\text{sk}}$  relative to  $\mathbf{M}^{\text{sk}}$ , such  $k$  provides for the existence of low-degree polynomials  $G_6$  and  $G_7$  where

$$\kappa(\mathbf{A}_k^{\text{sk}}) = \frac{\|\mathbf{A}_k^{\text{sk}}\|}{\sigma_{\min}(\mathbf{A}_k^{\text{sk}})} \leq \frac{\|\mathbf{R}^{\text{sk}}\|}{\|\mathbf{C}_{k-1}^{\text{sk}}\|} G_6(n) \leq G_7(n)\mathbf{u}^{-1}.$$

This bound can be used to show that  $\mathbf{M}_k$  is also numerically full-rank, in that

$$\kappa(\mathbf{M}_k) \leq \frac{1+\delta}{1-\delta} \kappa(\mathbf{S}\mathbf{M}_k) \lesssim \kappa(\mathbf{A}_k^{\text{sk}}) \leq G_7(n)\mathbf{u}^{-1}. \quad (14)$$

The first inequality in (14) holds due to the  $\delta$ -embedding property of  $\mathbf{S}$ . The second inequality can be shown through three steps:  $\kappa(\mathbf{A}_k^{\text{sk}}) \gtrsim \kappa(\mathbf{Q}_k^{\text{sk}} \mathbf{A}_k^{\text{sk}}) \gtrsim \kappa(\mathbf{M}_k^{\text{sk}}) \gtrsim \kappa(\mathbf{S}\mathbf{M}_k)$ , employing standard rounding bounds for matrix operations, with the fact that the left-hand-side matrix is numerically full rank (in steps two and three).

**Preconditioning and reconstruction error for leading columns.** The next step in the proof is to look at  $\mathbf{M}_k^{\text{pre}} \mathbf{A}_k^{\text{sk}}$  as an unpivoted “sketched CholeskyQR” decomposition of  $\mathbf{M}_k$ , in the sense of [Bal22]. According to [Bal22, Theorem 5.2], if  $\kappa(\mathbf{M}_k) \lesssim G_7(n)\mathbf{u}^{-1}$ , then there is a low-degree polynomial  $G_8$  for which

$$\|\mathbf{M}_k - \mathbf{M}_k^{\text{pre}} \mathbf{A}_k^{\text{sk}}\| \leq G_8(k)\mathbf{u}\|\mathbf{M}_k\| \quad \text{and} \quad \kappa(\mathbf{M}_k^{\text{pre}}) \lesssim \frac{1+\delta}{1-\delta}. \quad (15)$$

This establishes the condition number bound needed in (8). It also controls reconstruction error for the first  $k$  columns of  $\mathbf{M}_n$ .

**Reconstruction error for trailing columns.** To establish (8), it remains to bound the reconstruction error of the trailing  $n - k$  columns of  $\mathbf{M}$ . Toward this end, we adopt the notation that

$$\bar{\mathbf{M}}_k := \mathbf{M}[:, J[k+1:n]] \quad \text{and} \quad \bar{\mathbf{M}}_k^{\text{sk}} := \mathbf{M}^{\text{sk}}[:, J[k+1:n]].$$



By using the reconstruction error bound for  $\mathbf{M}_k$  from Eq. (15), the  $\delta$ -embedding property, standard bounds for matrix operations, and the reconstruction error bound for  $\mathbf{M}_k^{\text{sk}}$ , one finds that

$$\begin{aligned} \frac{\|\bar{\mathbf{M}}_k - \mathbf{M}_k^{\text{pre}} \mathbf{B}_k^{\text{sk}}\|}{\|\mathbf{M}\|} &\lesssim \frac{\|\bar{\mathbf{M}}_k - \mathbf{M}_k (\mathbf{A}_k^{\text{sk}})^{-1} \mathbf{B}_k^{\text{sk}}\|}{\|\mathbf{M}\|} \leq \frac{1 + \delta}{1 - \delta} \frac{\|\mathbf{S} \bar{\mathbf{M}}_k - \mathbf{S} \mathbf{M}_k (\mathbf{A}_k^{\text{sk}})^{-1} \mathbf{B}_k^{\text{sk}}\|}{\|\mathbf{S} \mathbf{M}\|} \\ &\lesssim \frac{1 + \delta}{1 - \delta} \frac{\|\bar{\mathbf{M}}_k^{\text{sk}} - \mathbf{M}_k^{\text{sk}} (\mathbf{A}_k^{\text{sk}})^{-1} \mathbf{B}_k^{\text{sk}}\|}{\|\mathbf{M}^{\text{sk}}\|} \lesssim \frac{1 + \delta}{1 - \delta} \frac{\|\bar{\mathbf{M}}_k^{\text{sk}} - \mathbf{Q}_k^{\text{sk}} \mathbf{B}_k^{\text{sk}}\|}{\|\mathbf{M}^{\text{sk}}\|}. \end{aligned} \quad (16)$$

Notably, the strong RRQR property of  $\mathbf{R}_k$  plays a key role in Eq. (16). It ensures that the terms of the form  $\|\mathbf{E}(\mathbf{A}_k^{\text{sk}})^{-1} \mathbf{B}_k^{\text{sk}}\|$ , for some error matrices such as  $\mathbf{E} = \mathbf{M}_k - \mathbf{M}_k^{\text{pre}} \mathbf{A}_k^{\text{sk}}$ , are bounded by  $g_k \|\mathbf{E}\|$ , and as such remain within machine precision.

We combine Eq. (16) with the stability of the `qrqp` routine and the criterion Eq. (13) used for selecting the truncation index  $k$  to get

$$\frac{\|\bar{\mathbf{M}}_k - \mathbf{M}_k^{\text{pre}} \mathbf{B}_k^{\text{sk}}\|}{\|\mathbf{M}\|} \lesssim \frac{1 + \delta}{1 - \delta} \frac{\|\bar{\mathbf{M}}_k^{\text{sk}} - \mathbf{Q}_k^{\text{sk}} \mathbf{B}_k^{\text{sk}}\|}{\|\mathbf{M}^{\text{sk}}\|} \lesssim \frac{1 + \delta}{1 - \delta} \frac{\|\mathbf{C}_k^{\text{sk}}\|}{\|\mathbf{R}_k^{\text{sk}}\|} \leq G_9(n)u. \quad (17)$$

This fulfills our need for a reconstruction error bound for the trailing columns of  $\mathbf{M}$ .

### 3.3 Determining numerical rank in practice

Here we suggest a flexible two-stage approach to numerical rank estimation. The general goal is to find the largest  $k$  where orthogonality loss can be bounded to within some specified tolerance. In the first stage, we overestimate  $k$  by a naive implementation of the `rank` function at Line 4. For example, one can set

$$k_o = \min\{\ell : \|\mathbf{C}_\ell^{\text{sk}}\|_{\text{F}} \leq us\}, \quad (18a)$$

where  $s$  is the maximum entry of  $|\mathbf{R}^{\text{sk}}|$ . This makes  $k_o$  cheap to compute and ensures  $\|\mathbf{C}_{k_o}^{\text{sk}}\|_2 \leq u \|\mathbf{R}^{\text{sk}}\|_2$ . The second stage begins by forming  $\mathbf{M}_{k_o}^{\text{pre}} = \text{TRSM}(\mathbf{M}_{k_o}, \mathbf{A}_{k_o}^{\text{sk}})$  and then computing the Cholesky factor  $\mathbf{R}^{\text{pre}}$  of the Gram matrix  $(\mathbf{M}_{k_o}^{\text{pre}})^* (\mathbf{M}_{k_o}^{\text{pre}})$ . It proceeds by using a function “`cond`” that estimates or bounds the condition number of an input matrix. Considering an orthogonality loss tolerance  $\epsilon_{\text{tol}}$  (say,  $\epsilon_{\text{tol}} = 100u$ ), it computes

$$k = \max\{\ell : \text{cond}(\mathbf{A}_\ell^{\text{pre}}) \leq \sqrt{u/\epsilon_{\text{tol}}}\}. \quad (18b)$$

This way, if `cond` always returns *upper bounds* on the condition numbers of input matrices, then CQRRPT’s returned Q-factor would have orthogonality loss of at most  $\mathcal{O}(\epsilon_{\text{tol}})$ .

Now we turn to the question of how to compute (18b) efficiently. For this, we impose a near-trivial requirement that `cond` satisfy  $\text{cond}(\mathbf{X}) \geq \text{cond}(\mathbf{Y})$  holds whenever  $\mathbf{Y}$  is a submatrix of  $\mathbf{X}$ . This lets us compute (18b) by binary search over  $\ell$  in  $\{1, \dots, k_o\}$ , rather than with linear search over the same. Of course, there is no need to recompute  $\mathbf{A}_\ell^{\text{pre}}$  from scratch at each iteration, since it is simply the leading  $\ell \times \ell$  submatrix of  $\mathbf{R}^{\text{pre}}$  for  $\ell \leq k_o$ . It is also important for `cond` to exploit structure in the provided input matrices. In particular, we only need to compute condition number estimates for matrices that are square, triangular, and that *typically* have most of their mass concentrated on their diagonal. Letting  $\mathbf{X}$  denote such a matrix, we could use  $\text{cond}(\mathbf{X}) = \kappa(\text{diag}(\mathbf{X}))$  to estimate  $\kappa(\mathbf{X})$  from below. Alternatively, we could bound  $\|\mathbf{X}\|_2$  and  $\|\mathbf{X}^{-1}\|_2$  from above with a Krylov subspace method of arithmetic complexity  $\mathcal{O}(n^2 \log n)$ . A similar Krylov subspace approach with half



the complexity could be used to compute a spectral norm estimate  $\tau \geq \|\mathbf{I} - \mathbf{X}\|_2$ , which can be turned around to bound  $\kappa(\mathbf{X}) \leq (1 + \tau)/(1 - \tau)$ . The last of these approaches is notable since if  $\mathbf{S}$  is a  $\delta$ -embedding for  $\text{range}(\mathbf{M})$  with a reasonable value of  $\delta$  (say,  $\delta < 0.99$ ) then an accurate spectral norm estimate  $\tau$  should satisfy  $\tau \lesssim \delta$ .

*Remark 1* (What if Cholesky fails?). Consider a scenario where  $\mathbf{G} = (\mathbf{M}_n^{\text{pre}})^*(\mathbf{M}_n^{\text{pre}})$  is such that the submatrix  $\mathbf{G}[1:k_o, 1:k_o]$  is positive-definite and  $\mathbf{G}[1:(k_o+1), 1:(k_o+1)]$  is not positive definite. Here, Cholesky factorization defined by LAPACK’s POTRF function will naturally fail. However, the leading  $k_o$ -by- $k_o$  submatrix of the output  $\mathbf{R}$  factor will be well-formed and satisfy  $(\mathbf{R}[1:k_o, 1:k_o])^*\mathbf{R}[1:k_o, 1:k_o] = \mathbf{G}[1:k_o, 1:k_o]$ . Therefore if POTRF fails at Line 6 and returns an error code  $k$  then we can take  $k_o = k - 1$  as an initial estimate for numerical rank. Note that as a corollary of this observation, there is no strict need for a numerical rank estimation step before the second phase of our two-phase approach.

## 4 Pivot quality experiments

The standard LAPACK function for QRCP, GEQP3, implements max-norm pivoting. This section gives experimental comparisons for the pivot quality of CQRRPT *based on* GEQP3, compared to the pivot quality of GEQP3 itself. Of course, the results of such a comparison depend heavily on the distribution family  $\mathcal{F}$  and the sampling factor  $\gamma$  that determines the distribution of our sketching operator. Therefore we take this as an opportunity to show how one might set  $\mathcal{F}$  and  $\gamma$  in practice. We particularly focus on the sparse sketching operators called SASOs from Section 2.3, since these are what we use in RandLAPACK’s CQRRPT implementation.

### 4.1 Background for pivot quality experiments

Some key concepts are needed to interpret the experimental results in this section. The first group of concepts concerns when a matrix is “easy” or “hard” to sketch via sparse sketching operators. The second group concerns computationally cheap measures of pivot quality.

**Leverage scores and matrix coherence.** Recall how Section 2.3 presented results on how  $\gamma$  can be chosen for various sketching operator families to achieve oblivious subspace embedding properties. The relevant result for SASOs, Theorem 7, provides worst-case bounds that are valuable in theoretical analysis. However, some subspaces are “easier to sketch” with SASOs than this result would suggest, in the sense that the subspace embedding property can reliably be obtained with a far smaller sampling factor or sparsity parameter.

*Leverage scores* are a useful concept for understanding when a subspace might be easy or hard to accurately sketch with SASOs. They quantify the extent to which a low-dimensional subspace aligns with coordinate subspaces [Mah11, DM16, DM21].

**Definition 11.** Let  $\mathbf{U}$  be an  $m \times n$  column-orthonormal matrix. The  $i^{\text{th}}$  leverage score of  $\text{range}(\mathbf{U})$  is the squared row-norm  $\|\mathbf{U}[i, :]\|_2^2$ .

Note that since columns of a wide SASO are independent of one another, we can permute its columns without changing its distribution. Note also that a column-permutation of a sketching operator  $\mathbf{S}$  can equivalently be viewed as a row-permutation of a data matrix  $\mathbf{M}$ , at least for purposes of computing a sketch  $\mathbf{SM}$ . This suggests that we do not care about the precise order of the leverage scores. Indeed, in many cases, it suffices to summarize leverage scores with another concept called *coherence*, a notion that essentially provides a condition number for random sampling algorithms [Mah11, DM16, DM21].

**Definition 12.** Let  $\mathbf{M}$  be an  $m \times n$  full rank matrix and let  $\mathbf{U}$  be an  $m \times n$  matrix whose columns form an orthonormal basis for  $\text{range}(\mathbf{M})$ . The coherence of  $\mathbf{M}$  is defined as:

$$\mu(\mathbf{M}) := m \max_{i \in \llbracket m \rrbracket} \|\mathbf{U}[i, :]\|_2^2.$$

It is well-documented in the literature that matrices with higher coherence are harder to sketch. This can be seen in our context in Sections 4.2 and 4.3, when we report on pivot quality for CQRRPT with SASO sketching applied to low coherence and high coherence matrices, respectively. For more information on leverage scores and coherence, we refer the reader to [AMT10, DMIMW12] and to [MDM<sup>+</sup>23, §6].

**Cheap measures of pivot quality.** This section makes use of two pivot quality metrics. These metrics are cheap to compute, and they do not require access to intermediate representations of the data matrix as GEQP3 runs.

Suppose QRCP gives us a decomposition  $\mathbf{M}_n = \mathbf{Q}\mathbf{R}$  where  $\mathbf{M}_n = \mathbf{M}[:, J]$ , following our notation from Section 1.6. We can canonically approximate  $\mathbf{M}_n$  by a *rank- $k$  truncation*

$$\mathbf{Q}_k \mathbf{R}_k \approx \mathbf{M}_n.$$

When using a unitarily invariant norm, the error of this truncation is given by a norm of the trailing submatrix  $\mathbf{C}_k$ :

$$\|\mathbf{M}_n - \mathbf{Q}_k \mathbf{R}_k\| = \|\mathbf{C}_k\|.$$

In view of this, our experiments visualize ratios of the trailing submatrix norms from GEQP3 to those from our algorithm based on GEQP3. Qualitatively, CQRRPT’s pivot choices are “good” if this ratio is close to one for all  $k$ .

Another cheap pivot quality metric is the ratios of  $r_{ii} := |\mathbf{R}[i, i]|$  to the singular values of  $\mathbf{M}$ . If  $\mathbf{R}$  comes from GEQP3 then this ratio can be quite bad in the worst case. Letting  $\sigma_i$  denote the  $i^{\text{th}}$  singular value of  $\mathbf{M}$ , this only guarantees that  $\phi_i := r_{ii}/\sigma_i$  is between  $(n(n+1)/2)^{-1/2}$  and  $2^{n-1}$  [Hig21]. Since there is a chance for large deviations, we plot  $r_{ii}/\sigma_i$  for our algorithm and GEQP3 separately (rather than plotting the ratio  $r_{ii}^{\text{qp3}}/r_{ii}^{\text{ours}}$ ).

## 4.2 Example low-coherence matrices

Here we consider tall  $m \times n$  matrices with  $m = 2^{17} = 131072$  and  $n = 2000$  whose spectrum falls into one of the two following categories.

- Matrices for which the first ten percent of their singular values are all equal to one and the rest are decaying polynomially down to  $1/\kappa(\mathbf{M}) = 10^{-10}$ .
- Matrices with a “staircase-shaped” spectrum, such that

$$\sigma_i(\mathbf{M}) = \begin{cases} 1 & \text{for } 1 \leq i \leq n/4 \\ 8 \cdot 10^{-10} & \text{for } n/4 + 1 \leq i \leq n/2 \\ 4 \cdot 10^{-10} & \text{for } n/2 + 1 \leq i \leq 3n/4 \\ 10^{-10} & \text{for } 3n/4 + 1 \leq i \leq n. \end{cases}$$

In both cases, the test matrix has a high enough condition number for CholeskyQR to fail if no preconditioning was used. We generate the singular vectors of these matrices by orthogonalizing the columns of matrices with iid Gaussian entries. Generating the *left* singular vectors in this way ensures that the matrices have low coherence.

Figures 1 and 2 visualize metrics of CQRRPT’s pivot quality for these matrices, when it is configured to use maximally aggressive dimension reduction via SASOs (sampling factor  $\gamma = 1$  and a single nonzero per column). See the figures’ captions for discussion.

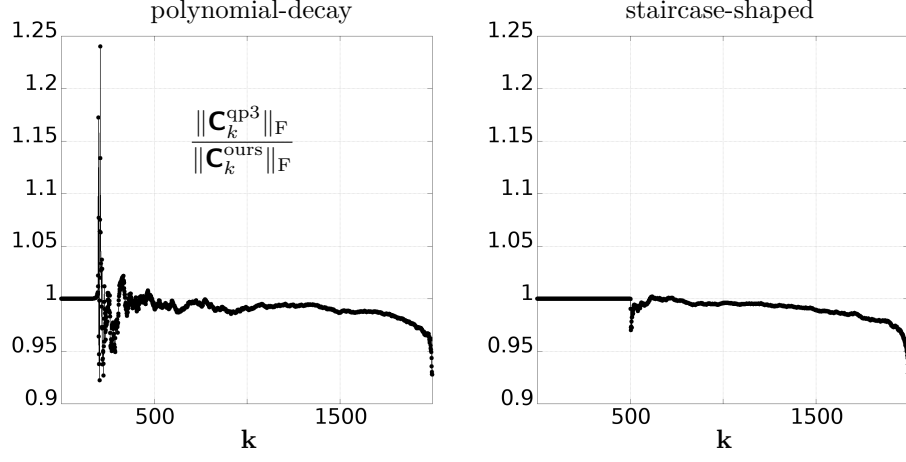


Figure 1: Ratios of **GEQP3**'s residual-norm metric to that of **CQRRPT** as a function of the truncation rank  $k$ . Our preferred outcome is that this ratio stays close to 1, and both plots bear this out. The left plot, featuring  $\mathbf{M}$  with a polynomially-decaying spectrum, first deviates from one around  $k = 200$ ; this is where the singular values of the data matrix begin decaying. The right plot, featuring  $\mathbf{M}$  with a staircase spectrum, deviates from one around  $k = 500$ ; this coincides with the location of the first drop in singular values. The lesson here is that **CQRRPT**'s pivots are more likely to differ from those of **GEQP3** at phase transitions of the spectrum.

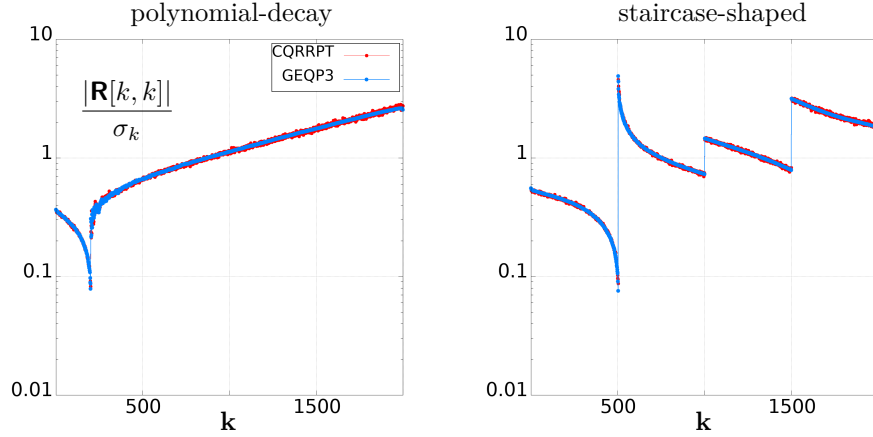


Figure 2: Plots for two matrices, each showing the ratios of the diagonal entries of  $|\mathbf{R}|$  (computed by **GEQP3** and **CQRRPT**) to the singular values of  $\mathbf{M}$  as a function of  $k$ . We expect *and see* that these curves for **CQRRPT** and **GEQP3** are extremely similar for both types of matrices. In fact, it is almost impossible to distinguish the curves for **CQRRPT** and **GEQP3** when these plots are rendered in grayscale. The message here is that even when the diagonal of  $\mathbf{R}$  from **GEQP3** and **CQRRPT** differ by larger margins (e.g., a factor 2), these differences can be immaterial in the broader context.

### 4.3 An example high-coherence matrix

Here we consider a matrix  $\mathbf{M}$  of the same dimensions as before,  $(m, n) = (131072, 2000)$ , constructed in three steps. The first step is to vertically stack  $c = \lfloor m/n \rfloor$  copies of the  $n \times n$  identity matrix and one copy of the first  $m - cn$  rows of the  $n \times n$  identity. The second step is to select  $n$  rows of  $\mathbf{M}$  at random and multiply them by  $10^{10}$ . Finally, the third step is to multiply  $\mathbf{M}$  on the right by a random  $n \times n$  orthogonal matrix. The left singular vectors are not explicitly generated in this matrix to ensure its high coherence.

Figure 3 shows pivot quality results when applying CQRRPT to  $\mathbf{M}$  with overly-aggressive dimension reduction; and Figure 4 shows the analogous data for more conservative dimension reduction. The figures' combined message is two-fold: that there is good reason to use  $\gamma > 1$  and more than one nonzero per column in  $\mathbf{S}$ , and that extensive parameter tuning is not needed to achieve reliable results from CQRRPT at low computational cost.

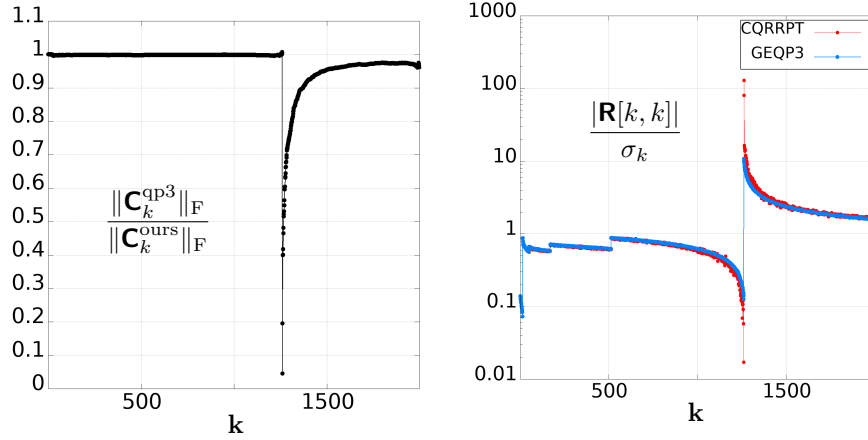


Figure 3: Pivot quality results for high-coherence  $\mathbf{M}$  when  $\gamma = 1$  and  $\text{nnz}(\mathbf{S}[:, i]) \equiv 1$ . Both plots show substantial degradation in the quality of CQRRPT's output around  $k \approx 1200$ .

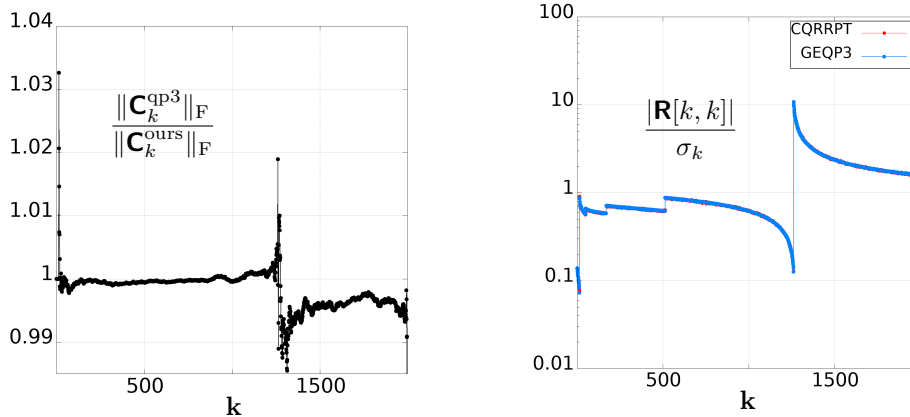


Figure 4: Pivot quality results for high-coherence  $\mathbf{M}$  when  $\gamma = 3$  and  $\text{nnz}(\mathbf{S}[:, i]) \equiv 4$ . The plots show that CQRRPT and GEQP3 produce nearly identical results.

## 5 Algorithm benchmarking

CQRRPT, together with its testing and benchmarking frameworks, have been implemented in the open-source C++ library called RandLAPACK. Together with its counterpart, RandBLAS, RandLAPACK provides a platform for developing, testing, and benchmarking of high-performance RandNLA algorithms. This software was developed as part of the BALLISTIC [DDL<sup>+</sup>20] project and is actively contributed to by the authors of this paper. All experiments in this section were run using the following version of our software:

<https://github.com/BallisticLA/RandLAPACK/releases/tag/CQRRPT-benchmark>.

The code for CQRRPT can be found in `/RandLAPACK/drivers/`. The code for constructing and dispatching the experiments can be found in `/benchmark/*`.

Experiments in this section are only concerned with algorithm speed. We measure speed in terms of either an algorithm’s canonical flop rate or wall clock time. The former metric is obtained by dividing the GEQRF flop count for a given matrix size (see [ADO94]) by the wall clock time required by a particular run of the algorithm. This metric helps in understanding how well different algorithms utilize the capabilities of a given machine.

The test matrices were generated with RandBLAS, by sampling each entry iid from the standard normal distribution. While these test matrices would not be suitable for assessing pivot quality, they are perfectly appropriate for speed benchmarks. All of our tests used double-precision arithmetic, all code was compiled with the `-O3` flag, and we use `OMP_NUM_THREADS = 48` unless otherwise stated. While using the maximum number of available threads may not always be the optimal approach to achieve peak algorithm performance, we advocate for harnessing all available computational resources. Algorithm engineering intricacies such as thread tuning are highly dependent on the specific hardware and fall beyond the scope of this paper.

We ran the experiments on a machine<sup>6</sup> with two Intel Xeon Gold 6248R processors; detailed configurations are listed in Table 1.

		Intel Xeon Gold 6248R (2x)
Cores per socket		24
Clock Speed	Base	3.00 GHz
	Boost	4.00 GHz
Cache sizes per socket	L1	1536 KB
	L2	24 MB
	L3	35.75 MB
RAM	Type	DDR4-2933
	Size	192 GB
BLAS & LAPACK		MKL 2023.2
GFLOPS in GEMM		1570

Table 1: Key configurations on hardware where testing was performed.

<sup>6</sup>a single node in ISAAC-NG [cluster](#)

## 5.1 CQRRPT versus other algorithms

Our first round of experiments compares CQRRPT to other algorithms for QR and QRCP. Specifically, we compare our algorithm to the following.

- GEQRF - standard unpivoted Householder QR.
- GEQR - unpivoted QR, which dispatches either a specialized algorithm for QR of tall and skinny matrices *or* a general-purpose algorithm according to implementation-specific logic. The selected algorithm is nominally based on a prediction of which algorithm will be more efficient for the given matrix. Intel MKL documentation does not promise that GEQR makes the optimal decision in this regard.
- GEQP3 - standard pivoted QR.
- GEQPT - composed of performing GEQR on an input matrix to get the factors  $\mathbf{Q}_1$  and  $\mathbf{R}_1$  and then getting data  $(\mathbf{Q}_2, \mathbf{R}, J)$  by running GEQP3 on  $\mathbf{R}_1$ ; the final matrix  $\mathbf{Q}$  is defined implicitly as the product of  $\mathbf{Q}_1$  and  $\mathbf{Q}_2$ .
- sCholQR3 - shifted CholeskyQR3, our implementation of [FKN<sup>+</sup>20, Algorithm 4.2], using the Frobenius norm on Line 3 of said algorithm.

The performance data for each algorithm is taken as the best of its execution times over twenty consecutive runs.

**Varying matrix sizes.** Our first set of experiments was run on  $m \times n$  matrices with  $m = 65536$  (Figure 5, left) and  $m = 131072$  (Figure 5, right), with  $n$  varying as the powers of two from 512 to 8192. The sampling factor,  $\gamma$ , is set to the default value of 1.25. Note that all matrices in this experiment are out of cache.

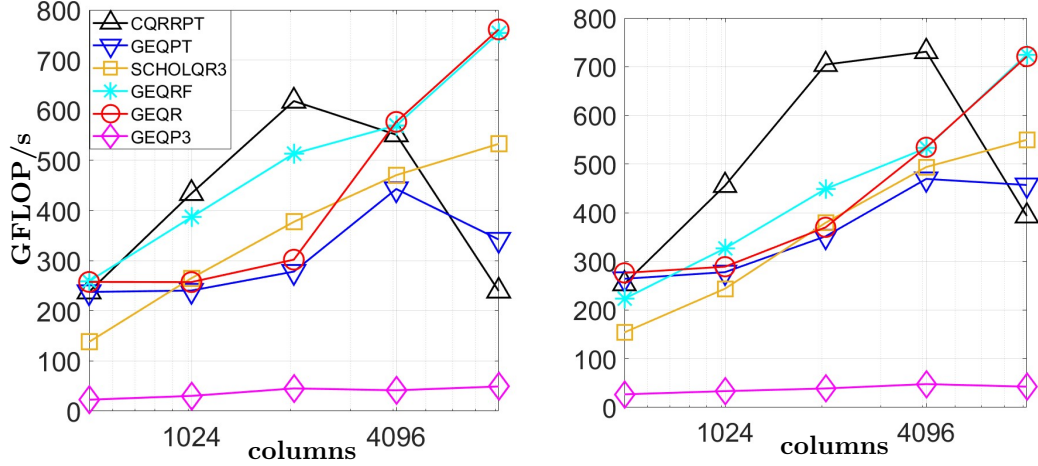


Figure 5: QR schemes performance comparisons for matrices with fixed numbers of rows ( $2^{16} = 65536$ , and  $2^{17} = 131072$  respectively) and varying numbers of columns (512, ..., 8192). In the case with 131072 rows, CQRRPT remains the fastest algorithm up until  $n = 8192$ ; at that point, operations on submatrices in underlying LAPACK routines no longer fit in the cache.

The results show that with an increase in input matrix size, CQRRPT outperforms alternative pivoted schemes and has either comparable or superior performance to unpivoted

schemes. We are seeing an order of magnitude acceleration over **GEQP3**, and accelerations of up to 2x over **GEQR** and **GEQPT**, and 1.6x over **GEQRF**, for matrices with 131072 rows. On a plot with 65536 rows, the performance of **CQRRPT** declines after 2048 columns due to the fact that the matrix is not tall enough.

Note that **GEQR** fails to match the performance of **GEQRF** and consequently causes poor performance in **GEQPT**. This is likely due to the fact that the matrix sizes that we use in our experiments are not considered “tall enough” by the internal metric of the MKL implementation of **GEQR**. For experiments with matrices where  $m$  is several orders of magnitude larger than  $n$ , we refer the readers to Appendix C.1.

**Varying number of threads.** Table 2 depicts the performance scaling of various algorithms with the change in number of threads used. For the dimensions of the test matrix used here, **CQRRPT** remains the fastest algorithm for any number of threads.

Threads	CQRRPT	GEQPT	sCholQR3	GEQRF	GEQR	GEQP3
8	250	159	147	121	166	21
16	490	286	276	274	300	25
24	577	351	316	343	369	29
36	677	372	388	411	393	50
48	704	351	379	448	370	39

Table 2: Performance (canonical GFLOP/s) scaling with the number of threads used, given  $\mathbf{M} \in \mathbb{R}^{131072 \times 2048}$ . Observe that at this particular input matrix size, **CQRRPT** outperforms all other listed algorithms.

It is worth noting that **CQRRPT** has an additional possible performance advantage over the alternative algorithms that come from the output format that **CQRRPT** uses. Namely, having an explicit representation of a **Q**-factor ensures that the factor can be applied via a fast **GEMM** function as opposed to a slower **ORMQR**, which is used to apply an implicitly-stored **Q**-factor. We acknowledge the existence of applications where having an implicitly stored **Q**-factor is a necessity (for example, when the full square **Q** is required). In the context of such applications, the output format of **CQRRPT** would be disadvantageous.

## 5.2 Profiling and optimizing CQRRPT

As seen from the pseudocode of Algorithm 2, **CQRRPT** consists of a handful of subcomponents. Understanding how each such subcomponent affects overall runtime for varying input parameters is important for potential future optimizations of **CQRRPT**. To give perspective on this, we present some timing data in Figure 6. As before, we use an  $m \times n$  Gaussian test matrix with  $m = 131072$  and  $n$  as powers of two from 32 to 16384. We also set the sampling factor,  $\gamma$ , to the default value of 1.25.

An immediate observation to be made here is that **QRCP** and **CholeskyQR** become the most time-consuming subroutines as the matrix size increases. Additionally, **QRCP** clearly becomes the main computational bottleneck. As the embedding dimension parameter affects the timing of **QRCP** greatly, it is important to understand how the choice of this parameter affects **CQRRPT**’s overall wall clock time.

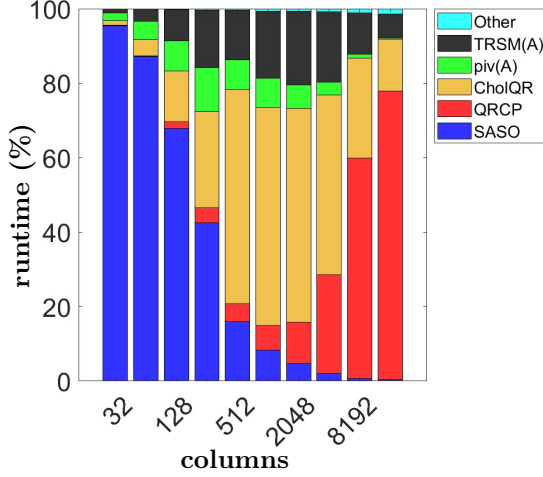


Figure 6: Percentages of CQRRPT's runtime, occupied by its respective sub-routines. Note that the cost of sketching becomes negligible for larger matrices. Note also that when  $d \geq n$ , the cost of applying QRCP to the  $d \times n$  sketch grows as  $\Omega(n^3)$ . By contrast, the cost of applying CholeskyQR to the  $m \times n$  preconditioned matrix grows as  $\mathcal{O}(mn^2)$ . Therefore, it is reasonable that QRCP consumes a larger fraction of runtime as  $n$  increases.

### 5.2.1 Effect of varying the embedding dimension parameter

Let's take a look at the effect of varying the embedding dimension in practice. We use Gaussian random input matrices of sizes  $131072 \times n$  for  $n \in \{1024, 2048, 4096\}$  with the ratio  $\gamma = d/n$  varying from 1 to 4 in steps of 0.5. Results are presented in Figure 7.

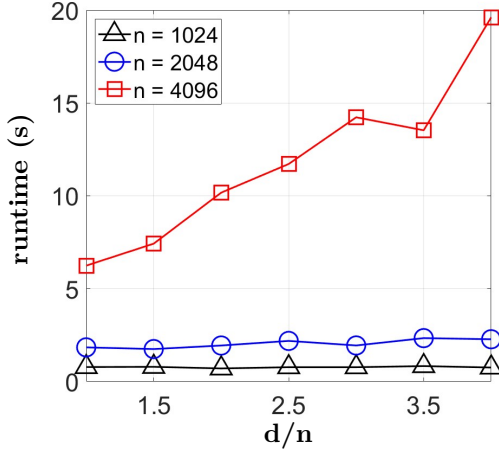


Figure 7: Effect of varying the embedding dimension for matrices of size  $131072 \times \{1024, 2048, 4096\}$ . Runtime represents the wall clock time for the full execution of CQRRPT. An increase of the embedding dimension has a larger effect on wider matrices, as QRCP becomes more expensive with the increased number of columns, as shown in Figure 6.

Note that for a smaller column size  $n$ , increasing the parameter  $\gamma$  has little to no effect on CQRRPT's overall runtime, as the portion of runtime dedicated to performing the QRCP on a sketch is smaller. However, as the figure suggests, for a larger  $n = 4096$ , the effect of increasing  $\gamma$  is rather noticeable. Recalling our results from Section 4.2, small  $\gamma$  can still guarantee accurate results for matrices of low coherence, therefore, a good starting point for the value of this parameter would be somewhere between one and two in such cases.

### 5.2.2 Performing HQRRP on the sketch

By now we have repeatedly seen that CQRRPT's method for QRCP of  $\mathbf{M}^{\text{sk}}$  can decisively impact its runtime when  $n$  is large. Here we explore the possibility of accelerating this operation by replacing CQRRPT's call to GEQP3 with a call to HQRRP (Householder QR



Factorization With Randomization for Pivoting, see [MQOHvdG17]). As outlined in Section 1.4, HQRRP uses low-dimensional random projections to make pivot decisions in small blocks.

We have ported an existing implementation of HQRRP into RandLAPACK and first ran experiments comparing HQRRP to GEQP3 directly. In these experiments, we used rectangular matrices of sizes  $n \times n$  for  $n \in \{1000, 2000, \dots, 10000\}$  with varying number of OpenMP threads used (which also sets the number of threads used by Intel MKL). Another important tuning parameter to consider in HQRRP benchmarking is the block size. Upon experimenting with different HQRRP block sizes, we have concluded that on our particular system, using the block size of 32 results in the best performance for HQRRP. Using other block sizes in  $\{8, 16, 64, 128, 256\}$  resulted in worse performance relative to what we report in this paper. Results are presented in Figure 8.

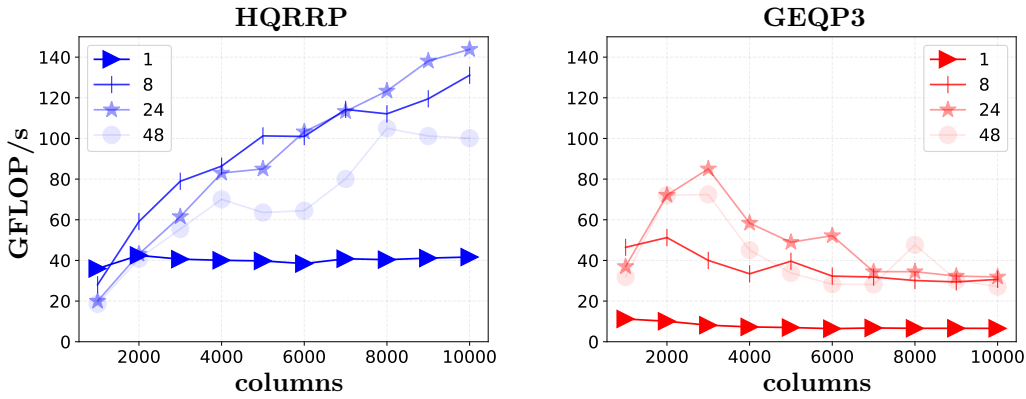


Figure 8: Canonical flop rates for HQRRP vs GEQP3 with `OMP_THREADS` in  $\{1, 8, 24, 48\}$ . The experimental speedup of HQRRP over GEQP3 for the larger matrix sizes is significant, but it does not match the speedup reported in [MQOHvdG17]; this may be due to a variety of factors (primarily, the machine used for benchmarking).

As seen in Figure 8, HQRRP achieves its peak performance with 24 threads for large matrix sizes, undoubtedly beating the performance of GEQP3. However, for small input matrices, using a large number of threads results in HQRRP failing to outperform GEQP3. When 48 threads are used, the performance of HQRRP stagnates, similar to other QR factorization algorithms; see Appendix C.2 for an explanation of why this happens.

Figure 8 allows us to conclude that it is preferred to use 8 threads when running HQRRP on the matrices with  $n \leq 6000$ ; using 24 threads would be optimal for matrices of larger sizes. Additionally, using 24 threads should result in the best performance of GEQP3. Assuming CQRRPT used ideal parameter choices for HQRRP and GEQP3 on our machine, we would expect the HQRRP version to outperform the GEQP3 version when  $n \geq 3000$ .

## 6 Conclusion

This paper introduces CQRRPT, a randomized algorithm for computing a QRCP factorization of a tall matrix. The algorithm consists of two ingredients: obtaining the pivot order and an approximate R-factor from a small random sketch; and retrieving the complete QRCP factorization by a preconditioned CholeskyQR. In comparison to standard QR algorithms, such as Householder QR, TSQR, and their pivoted (possibly randomized) derivatives, our

CQRRPT requires  $\frac{4}{3}$ x less flops<sup>7</sup> and is better suited to modern computational architectures due to fewer global synchronization points, fewer data passes, and/or more straightforward reduction operator. Notably, CQRRPT provides unconditional numerical stability, in contrast to existing sketched QR, and CholeskyQR methods. This makes the algorithm an appealing tool for orthogonalization.

We established rigorous conditions for the random sketch required by CQRRPT to attain the rank-revealing property and numerical stability. These conditions can be met by employing a sketching operator that possesses oblivious subspace embedding property. The robustness and performance advantages of CQRRPT were confirmed through extensive numerical experiments of a RandLAPACK implementation based on RandBLAS. In particular, we observed flop rates improvements of up to 10x compared to the standard pivoted QR routine GEQP3 and 1.4x compared to the unpivoted QR routine GEQRF from LAPACK.

This paper also highlights several promising research directions. First, the stability requirements and the efficiency of CQRRPT in certain scenarios can be improved by using more sophisticated sketching operators and schemes for computing the sketch-orthonormal preconditioned matrix. The performance of CQRRPT in modern computing environments such as GPUs, distributed systems, and multi-(or low-)precision arithmetic systems also remains to be explored. Second, combining our theoretical results from Appendix A with the analysis from [XGL17] may lead to a deeper understanding of the properties of HQRRP and other RandNLA methods existing or yet to emerge. Third, CQRRPT can be extended to be applicable to matrices with any aspect ratio by integrating ideas from this paper with ideas from [XGL17, DG17, Mar15, MQOHvdG17] for HQRRP and the related randomized and communication-avoiding QR techniques.

## Acknowledgements

This work was partially funded by an NSF Collaborative Research Framework: Basic ALgebra Libraries for Sustainable Technology with Interdisciplinary Collaboration (BALLISTIC), a project of the International Computer Science Institute, the University of Tennessee’s ICL, the University of California at Berkeley, and the University of Colorado at Denver (NSF Grant Nos. 2004235, 2004541, 2004763, 2004850, respectively). MWM would also like to acknowledge the NSF, DOE, and ONR Basic Research Challenge on RLA for providing partial support for this work. RM’s contributions to this work were made before joining Sandia, when he held affiliations with ICSI, UC Berkeley, and LBNL.

## References

- [ADO94] E. Anderson, J. Dongarra, and S. Ostrouchov, *LAPACK working note 41 installation guide for LAPACK*, Technical Report 37996-1301, 1994.
- [AMT10] H. Avron, P. Maymounkov, and S. Toledo, *Blendepik: Supercharging LAPACK’s Least-Squares Solver*, SIAM Journal on Scientific Computing **32** (January 2010), no. 3, 1217–1236.
- [Bal22] O. Balabanov, *Randomized Cholesky QR factorizations*, arXiv, 2022.
- [BG21] O. Balabanov and L. Grigori, *Randomized block gram-schmidt process for solution of linear systems and eigenvalue problems*, arXiv, 2021.
- [BG22] ———, *Randomized Gram–Schmidt process with application to GMRES*, SIAM Journal on Scientific Computing **44** (2022), no. 3, A1450–A1474.
- [BG65] P. Businger and G. Golub, *Linear least squares solutions by Householder transformations*, Numerische Mathematik **7** (1965), 269–276.

---

<sup>7</sup>to compute QRCP factorization in explicit form

- [Bjö96] Åke Björk, *Numerical methods for least squares problems*, SIAM, 1996. ISBN 0-89871-360-9.
- [Coh16] M.B. Cohen, *Nearly tight oblivious subspace embeddings by trace inequalities*, Proceedings of the 27th annual ACM-SIAM Symposium on Discrete Algorithms, December 2016.
- [DDL<sup>+</sup>20] J. Demmel, J. Dongarra, J. Langou, J. Langou, P. Luszczek, and M.W. Mahoney, *Prospectus for the next LAPACK and ScaLAPACK libraries: Basic ALgebra Llibraries for Sustainable Technology with Interdisciplinary Collaboration (BALLISTIC)*, 2020.
- [Dem23] J. Demmel, *Nearly optimal block-Jacobi preconditioning*, SIAM Journal on Matrix Analysis and Applications **44** (March 2023), no. 1, 408–413.
- [DG17] J.A. Duersch and M. Gu, *Randomized QR with column pivoting*, SIAM Journal on Scientific Computing **39** (January 2017), no. 4, C263–C291.
- [DGHL12] J. Demmel, L. Grigori, M. Hoemmen, and J. Langou, *Communication-optimal parallel and sequential QR and LU factorizations*, SIAM Journal on Scientific Computing **34** (2012), no. 1, A206–A239.
- [DM16] P. Drineas and M. W. Mahoney, *RandNLA: Randomized numerical linear algebra*, Communications of the ACM **59** (2016), 80–90.
- [DM21] M. Derezhinski and M. W. Mahoney, *Determinantal point processes in randomized numerical linear algebra*, Notices of the AMS **68** (2021), no. 1, 34–45.
- [DMIMW12] P. Drineas, M. Magdon-Ismail, M. W. Mahoney, and D. P. Woodruff, *Fast approximation of matrix coherence and statistical leverage*, Journal of Machine Learning Research **13** (2012), 3475–3506.
- [DMM06] P. Drineas, M. W. Mahoney, and S. Muthukrishnan, *Sampling algorithms for  $\ell_2$  regression and applications*, Proceedings of the 17th annual ACM-SIAM Symposium on Discrete Algorithms (SODA), 2006, pp. 1127–1136.
- [DMMS11] P. Drineas, M. W. Mahoney, S. Muthukrishnan, and T. Sarlós, *Faster least squares approximation*, Numerische Mathematik **117** (2011), no. 2, 219–249.
- [FGL21] Y. Fan, Y. Guo, and T. Lin, *A novel randomized XR-based preconditioned CholeskyQR algorithm*, arXiv, 2021.
- [FKN<sup>+</sup>20] T. Fukaya, R. Kannan, Y. Nakatsukasa, Y. Yamamoto, and Y. Yanagisawa, *Shifted Cholesky QR for computing the QR factorization of ill-conditioned matrices*, SIAM Journal on Scientific Computing **42** (2020), no. 1, A477–A503 (cit. on pp. 2, 19, 20).
- [FNYY14] T. Fukaya, Y. Nakatsukasa, Y. Yanagisawa, and Y. Yamamoto, *Choleskyqr2: A simple and communication-avoiding algorithm for computing a tall-skinny QR factorization on a large-scale parallel system*, 2014 5th workshop on latest advances in scalable algorithms for large-scale systems, 2014, pp. 31–38.
- [GE96] M. Gu and S.C. Eisenstat, *Efficient algorithms for computing a strong rank-revealing QR factorization*, SIAM Journal on Scientific Computing **17** (July 1996), no. 4, 848–869.
- [GVL13] G.H. Golub and C.F. Van Loan, *Matrix computations*, 4th ed., Johns Hopkins Studies in the Mathematical Sciences, Johns Hopkins University Press, Baltimore, MD, 2013 (en).
- [Hig02] N.J. Higham, *Accuracy and stability of numerical algorithms*, Second, Society for Industrial and Applied Mathematics, Philadelphia, PA, USA, 2002.
- [Hig21] ———, *What is a rank-revealing factorization?*, 2021. [Accessed 03-Apr-2023].
- [Hig22] ———, *The big six matrix factorizations—nhigham.com*, 2022. [Accessed 15-Mar-2023].
- [HSBY23] Andrew J. Higgins, Daniel B. Szyld, Erik G. Boman, and Ichitaro Yamazaki, *Analysis of randomized Householder-Cholesky QR factorization with multisketching*, 2023. arXiv:2309.05868.
- [Mah11] M. W. Mahoney, *Randomized algorithms for matrices and data*, Foundations and Trends in Machine Learning, NOW Publishers, Boston, 2011.
- [Mar15] P.-G. Martinsson, *Blocked rank-revealing QR factorizations: How randomized sampling can be used to avoid single-vector pivoting*, arXiv preprint arXiv:1505.08115 (2015).
- [MDM<sup>+</sup>23] R. Murray, J. Demmel, M.W. Mahoney, N.B. Erichson, M. Melnichenko, O.A. Malik, L. Grigori, P. Luszczek, M. Derezhinski, M.E. Lopes, T. Liang, H. Luo, and J. Dongarra, *Randomized numerical linear algebra: A perspective on the field with an eye to software*, 2023. arXiv:2302.11474v2.

- [MQOHvdG17] P.-G. Martinsson, G. Quintana-Ortí, N. Heavner, and R. van de Geijn, *Householder QR factorization with randomization for column pivoting (HQRPP)*, SIAM Journal on Scientific Computing **39** (January 2017), no. 2, C96–C115.
- [MSM14] X. Meng, M.A. Saunders, and M.W. Mahoney, *LSRN: A parallel iterative solver for strongly over- or underdetermined systems*, SIAM Journal on Scientific Computing **36** (January 2014), no. 2, C95–C118.
- [MT20] P.-G. Martinsson and J. A. Tropp, *Randomized numerical linear algebra: Foundations and algorithms*, Acta Numerica **29** (2020), 403–572.
- [ND15] Hong Diep Nguyen and James Demmel, *Reproducible tall-skinny QR*, 2015 IEEE 22nd symposium on computer arithmetic, 2015, pp. 152–159.
- [QOSB98] G. Quintana-Ortí, X. Sun, and C.H. Bischof, *A BLAS-3 version of the QR factorization with column pivoting*, SIAM Journal on Scientific Computing **19** (1998), no. 5, 1486–1494.
- [RT08] V. Rokhlin and M. Tygert, *A fast randomized algorithm for overdetermined linear least-squares regression*, Proceedings of the National Academy of Sciences **105** (September 2008), no. 36, 13212–13217.
- [Sar06] T. Sarlos, *Improved approximation algorithms for large matrices via random projections*, Proceedings of the 47th annual IEEE Symposium on Foundations of Computer Science (FOCS), 2006, pp. 143–152.
- [Slu69] A. Van Der Sluis., *Condition numbers and equilibration of matrices.*, Numerische Mathematik **14** (1969), 14–23.
- [SW02] A. Stathopoulos and K. Wu, *A block orthogonalization procedure with constant synchronization requirements*, SIAM J. Sci. Comput. **23** (2002), 2165–2182.
- [TOO20] T. Terao, K. Ozaki, and T. Ogita, *LU-Cholesky QR algorithms for thin QR decomposition*, Parallel Computing **92** (2020), 102571.
- [TRG05] Rajeev Thakur, Rolf Rabenseifner, and William Gropp, *Optimization of collective communication operations in MPICH*, The International Journal of High Performance Computing Applications **19** (2005), no. 1, 49–66.
- [Tro11] J.A. Tropp, *Improved analysis of the subsampled randomized Hadamard transform*, Advances in Adaptive Data Analysis **03** (April 2011), no. 01n02, 115–126.
- [TW23] Joel A. Tropp and Robert J. Webber, *Randomized algorithms for low-rank matrix approximation: Design, analysis, and applications*, 2023.
- [Woo14] D.P. Woodruff, *Sketching as a tool for numerical linear algebra*, Found. Trends Theor. Comput. Sci. **10** (October 2014), no. 1–2, 1–157.
- [XGL17] J. Xiao, M. Gu, and J. Langou, *Fast parallel randomized QR with column pivoting algorithms for reliable low-rank matrix approximations*, 2017 IEEE 24th international conference on high performance computing (HiPC), 2017, pp. 233–242.
- [YNYF15] Y. Yamamoto, Y. Nakatsukasa, Y. Yanagisawa, and T. Fukaya, *Roundoff error analysis of the CholeskyQR2 algorithm*, Electron. Trans. Numer. Anal **44** (2015), no. 01, 306–326.
- [YTD15] I. Yamazaki, S. Tomov, and J. Dongarra, *Mixed-precision Cholesky QR factorization and its case studies on multicore CPUs with multiple GPUs*, SIAM J. Scientific Computing **37** (2015), C307–C330.

## A Algorithm analysis

Subspace embedding distortion is a ubiquitous concept in RandNLA theory. However, the results we have stated for CQRPP concern restricted singular values. The connection between restricted singular values and subspace embedding distortion can be seen with the help of the following concept.

**Definition 13.** *The effective distortion of  $\mathbf{S}$  for  $L$  is the minimum distortion that any sketching operator  $t\mathbf{S}$  can achieve for  $L$ , when we let ourselves optimize over  $t \geq 0$ .*

The specific connection is as follows [MDM<sup>+</sup>23, Proposition A.1.1].

**Proposition 14.** Suppose the columns of  $\mathbf{U}$  are an orthonormal basis for  $L = \text{range}(\mathbf{M})$ , and let  $\delta$  denote the effective distortion of  $\mathbf{S}$  for  $L$ . If  $\delta < 1$ , then we have

$$\kappa(\mathbf{S}\mathbf{U}) = \frac{1 + \delta}{1 - \delta}.$$

Furthermore, we have  $\delta = 1$  if and only if  $\text{rank}(\mathbf{S}\mathbf{M}) < \text{rank}(\mathbf{M})$ .

We use Proposition 14 to prove Theorems 1 and 2 (§A.1) and Theorems 3 and 4 (§A.3).

## A.1 Correctness and effect of preconditioning

*Proof of Theorem 1.* Let us begin by setting  $k = \text{rank}(\mathbf{M}^{\text{sk}})$ . Our assumptions on QRCP's semantics imply that we can take  $\mathbf{Q}^{\text{sk}}$  and  $\mathbf{R}^{\text{sk}}$  to be  $m \times k$  and  $k \times n$ , respectively. Following the notation from Section 1.6, we work with  $\mathbf{M}_\ell = \mathbf{M}[:, J[1:\ell]]$  for  $\ell = k$  and  $\ell = n$ . We express the  $m \times k$  matrix  $\mathbf{M}^{\text{pre}}$  from Algorithm 2 as  $\mathbf{M}^{\text{pre}} = \mathbf{M}_k(\mathbf{R}^{\text{sk}}[:, 1:k])^{-1}$ , and we denote the factors from its QR decomposition by  $\mathbf{Q}_k$  and  $\mathbf{R}^{\text{pre}}$ . Recall that the triangular factor returned by Algorithm 2 is  $\mathbf{R}_k = \mathbf{R}^{\text{pre}}\mathbf{R}^{\text{sk}}$ . In light of Proposition 14, the theorem's claim is that if  $\text{rank}(\mathbf{M}) = k$  then  $\mathbf{M}_n = \mathbf{Q}_k\mathbf{R}_k$ .

The proof rests on the identities  $\mathbf{Q}_k\mathbf{R}_k = \mathbf{M}^{\text{pre}}\mathbf{R}^{\text{sk}}$  and  $\mathbf{S}\mathbf{M}_n = \mathbf{S}\mathbf{M}^{\text{pre}}\mathbf{R}^{\text{sk}}$  which hold by construction. From the former identity we see that our task reduces to showing  $\mathbf{M}_n = \mathbf{M}^{\text{pre}}\mathbf{R}^{\text{sk}}$ , and toward this end we introduce  $\mathbf{\Delta} = \mathbf{M}_n - \mathbf{M}^{\text{pre}}\mathbf{R}^{\text{sk}}$ . We trivially have that  $\text{range}(\mathbf{\Delta}) \subset \text{range}(\mathbf{M})$ , and we need to show that  $\text{rank}(\mathbf{M}) = \text{rank}(\mathbf{S}\mathbf{M})$  implies  $\mathbf{\Delta} = \mathbf{0}$ . This is where the latter identity comes into play. Simply rewrite it as  $\mathbf{S}\mathbf{\Delta} = \mathbf{0}$  to see that  $\text{range}(\mathbf{\Delta}) \subset \ker(\mathbf{S})$ . At the same time, we know that  $\text{rank}(\mathbf{S}\mathbf{M}) = \text{rank}(\mathbf{M})$  implies  $\ker(\mathbf{S}) \cap \text{range}(\mathbf{M})$  is trivial. Combining these facts shows that  $\mathbf{\Delta} = \mathbf{0}$  when  $\text{rank}(\mathbf{M}) = k$ .  $\square$

*Proof of Theorem 2.* Let  $\mathbf{U}$  be an  $m \times k$  matrix whose columns are an orthonormal basis for  $\text{range}(\mathbf{M})$ , and let  $\mathcal{U}_i$  denote the set of  $i$ -dimensional subspaces of  $\mathbb{R}^k$ . The min-max principle offers the following expressions for the  $i^{\text{th}}$ -largest singular value of  $\mathbf{M}^{\text{pre}}$  and the  $i^{\text{th}}$ -smallest singular value of  $\mathbf{S}\mathbf{U}$ :

$$\sigma_i(\mathbf{M}^{\text{pre}}) = \min_{X \in \mathcal{U}_i} \max_{\mathbf{x} \in X} \frac{\|\mathbf{M}^{\text{pre}}\mathbf{x}\|_2}{\|\mathbf{x}\|_2} \quad \text{and} \quad \sigma_{k-i+1}(\mathbf{S}\mathbf{U}) = \max_{Y \in \mathcal{U}_i} \min_{\mathbf{y} \in Y} \frac{\|\mathbf{S}\mathbf{U}\mathbf{y}\|_2}{\|\mathbf{y}\|_2}.$$

Our goal is to show that  $\sigma_i(\mathbf{M}^{\text{pre}}) = (\sigma_{k-i+1}(\mathbf{S}\mathbf{U}))^{-1}$ . To do this, we assume the restricted singular values of  $\mathbf{S}$  on  $\text{range}(\mathbf{M})$  are all nonzero. This ensures that  $\text{range}(\mathbf{M}^{\text{pre}}) = \text{range}(\mathbf{M})$  and subsequently that there is an invertible matrix  $\mathbf{T}$  where  $\mathbf{M}^{\text{pre}} = \mathbf{U}\mathbf{T}$ . We also rely on the fact that the  $d \times k$  matrix  $\mathbf{S}\mathbf{M}^{\text{pre}}$  is column-orthonormal. Using this latter fact together with the factored representation of  $\mathbf{M}^{\text{pre}}$  gives a chain of identities

$$\sigma_i(\mathbf{M}^{\text{pre}}) = \min_{X \in \mathcal{U}_i} \max_{\mathbf{x} \in X} \frac{\|\mathbf{M}^{\text{pre}}\mathbf{x}\|_2}{\|\mathbf{x}\|_2} = \min_{X \in \mathcal{U}_i} \max_{\mathbf{x} \in X} \frac{\|\mathbf{M}^{\text{pre}}\mathbf{x}\|_2}{\|\mathbf{S}\mathbf{M}^{\text{pre}}\mathbf{x}\|_2} = \min_{X \in \mathcal{U}_i} \max_{\mathbf{x} \in X} \frac{\|\mathbf{U}\mathbf{T}\mathbf{x}\|_2}{\|\mathbf{S}\mathbf{U}\mathbf{T}\mathbf{x}\|_2}.$$

Then we apply a change of variables  $\mathbf{y} = \mathbf{T}\mathbf{x}$  to get

$$\sigma_i(\mathbf{M}^{\text{pre}}) = \min_{X \in \mathcal{U}_i} \max_{\mathbf{x} \in X} \frac{\|\mathbf{T}\mathbf{x}\|_2}{\|\mathbf{S}\mathbf{U}\mathbf{T}\mathbf{x}\|_2} = \min_{Y \in \mathcal{U}_i} \max_{\mathbf{y} \in Y} \frac{\|\mathbf{y}\|_2}{\|\mathbf{S}\mathbf{U}\mathbf{y}\|_2} = \left( \max_{Y \in \mathcal{U}_i} \min_{\mathbf{y} \in Y} \frac{\|\mathbf{S}\mathbf{U}\mathbf{y}\|_2}{\|\mathbf{y}\|_2} \right)^{-1}$$

which completes the proof.  $\square$

## A.2 Detailed arithmetic complexity analysis

In an effort to give the reader a perspective on an approximate flop count of Algorithm 2, let us take a closer look at what happens inside of this algorithm.

1. Define a sketching operator and compute a sketch. The cost of this step will vary greatly between types of sketching operators used. Overall, for a serious implementation suited for large data matrices, it should be negligible compared to the cost of later steps. We will denote the flop count of performing this step with  $C_{sk}$ .
2. Factor  $\mathbf{M}^{sk}$  by QRCP. The cost of this step depends on the algorithm used for QRCP. By default, we use the method from LAPACK's GEQP3. With LAPACK's GEQP3, this operation would cost  $4dnk - 2k^2(d+n) + 4k^3/3$  flops [GVL13, Algorithm 5.4.1], where  $k = \text{rank}(\mathbf{M}^{sk})$  and  $d$  is the user-defined embedding dimension of a sketch.
3. Apply the preconditioner to  $\mathbf{M}$ , to get  $\mathbf{M}^{pre}$ . This step is done via TRSM, so the cost is  $mk^2$  [ADO94, Page 120].
4. Run CholeskyQR on  $\mathbf{M}^{pre}$ . This operation is composed of SYRK, POTRF, and TRSM functions. This operation would cost  $mk(k+1) + k^3/3 + k^2/2 + k/6 + mk^2$  flops [ADO94, Page 120].
5. Combine the triangular factors from QRCP on  $\mathbf{M}^{sk}$  and CholeskyQR on  $\mathbf{M}^{pre}$ . This cost is negligible; an  $\mathcal{O}(n^3)$  TRMM.

This results in a cumulative flop count of  $2mk^2 + mk(k+1) + 4dnk - 2k^2(d+n) + 5k^3/3 + k^2/2 + k/6 + C_{sk}$ . Put simply, we have an algorithm with an asymptotic flop count with a leading term  $3mn^2$  for a full-rank data matrix.

## A.3 Rank-revealing properties

Here we prove pivot quality results claimed in Theorems 3 and 4. Nearly all of the work is to establish a proposition that relates (1) the spectra of  $\mathbf{M}$  and  $\mathbf{M}^{sk}$  as well as (2) the spectra of (submatrices of) R-factors from unpivoted QR of  $\mathbf{M}_n := \mathbf{M}[:, J]$  and  $\mathbf{M}_n^{sk} := \mathbf{M}^{sk}[:, J]$ , for an arbitrary pivot vector  $J$ . Henceforth, let us such a pivot vector and consider the thin QR factorizations  $\mathbf{Q}\mathbf{R}$  and  $\mathbf{Q}^{sk}\mathbf{R}^{sk}$  of  $\mathbf{M}_n$  and  $\mathbf{M}_n^{sk}$ , respectively. Note that the claims in Theorems 3 and 4 are vacuous if the restricted condition number for  $\mathbf{S}$  on  $\text{range}(\mathbf{M})$  is infinite. Therefore in proving them can assume that  $\text{rank}(\mathbf{M}) = \text{rank}(\mathbf{S}\mathbf{M}) = k$ . We use our standard notation from Section 1.6 for submatrices  $(\mathbf{A}_\ell, \mathbf{B}_\ell, \mathbf{C}_\ell)$  and  $(\mathbf{A}_\ell^{sk}, \mathbf{B}_\ell^{sk}, \mathbf{C}_\ell^{sk})$ .

**Proposition 15.** *If  $\mathbf{S}$  has effective distortion  $\delta < 1$  for the range of  $\mathbf{M}$ , then we have*

$$\frac{\sigma_j(\mathbf{A}_\ell)}{\sigma_j(\mathbf{M})} \geq \left( \frac{1-\delta}{1+\delta} \right) \frac{\sigma_j(\mathbf{A}_\ell^{sk})}{\sigma_j(\mathbf{M}^{sk})} \quad \text{for } j \leq \ell \quad (19a)$$

$$\frac{\sigma_j(\mathbf{C}_\ell)}{\sigma_{\ell+j}(\mathbf{M})} \leq \left( \frac{1+\delta}{1-\delta} \right) \frac{\sigma_j(\mathbf{C}_\ell^{sk})}{\sigma_{\ell+j}(\mathbf{M}^{sk})} \quad \text{for } j \leq k-\ell, \quad (19b)$$

$$\text{and} \quad \|(\mathbf{A}_\ell)^{-1}\mathbf{B}_\ell\|_2 \leq \|(\mathbf{A}_\ell^{sk})^{-1}\mathbf{B}_\ell^{sk}\|_2 + \left( \frac{1+\delta}{1-\delta} \right) \sigma_{\min}(\mathbf{A}_\ell^{sk})^{-1} \|\mathbf{C}_\ell^{sk}\|_2. \quad (19c)$$

*Proof.* First, note that all of our claimed bounds are invariant under scaling of  $\mathbf{S}$  by positive constants. This means that we can assume  $\mathbf{S}$  is scaled ( $\mathbf{S} \leftarrow t\mathbf{S}$  for some  $t \neq 0$ ) so that its distortion and its effective distortion coincide. From here, it follows directly from the min-max principle and the subspace embedding property of  $\mathbf{S}$  that

$$(1 - \delta)\sigma_j(\mathbf{M}) \leq \sigma_j(\mathbf{SM}) \leq (1 + \delta)\sigma_j(\mathbf{M}) \text{ for } 1 \leq j \leq n. \quad (20)$$

Consider the matrix  $\mathbf{M}^{\text{pre}}$  computed in Algorithm 2. We can interpret Theorem 2 with the definition of a subspace embedding to find that

$$(1 + \delta)^{-1} \leq \sigma_j(\mathbf{M}^{\text{pre}}) \leq (1 - \delta)^{-1} \text{ for } 1 \leq j \leq k. \quad (21)$$

Next, partition the matrix  $\mathbf{R}^{\text{pre}}$  from Algorithm 2 into a  $2 \times 2$  block matrix in the way analogous to the partitioning of  $\mathbf{R}$  and  $\mathbf{R}^{\text{sk}}$ , and recall the definition  $\mathbf{R} = \mathbf{R}^{\text{pre}}\mathbf{R}^{\text{sk}}$ .

The bounds in Eq. (21) ensure that  $\sigma_{\min}(\mathbf{A}_{\ell}^{\text{pre}}) \geq \sigma_{\min}(\mathbf{R}^{\text{pre}}) = \sigma_{\min}(\mathbf{M}^{\text{pre}}) \geq (1 + \delta)^{-1}$  and  $\|\mathbf{C}_{\ell}^{\text{pre}}\| \leq \|\mathbf{R}^{\text{pre}}\| = \|\mathbf{M}^{\text{pre}}\| \leq (1 - \delta)^{-1}$ . Meanwhile, rote calculations let us express the blocks of  $\mathbf{R}$  as  $\mathbf{A}_{\ell} = \mathbf{A}_{\ell}^{\text{pre}}\mathbf{A}_{\ell}^{\text{sk}}$ ,  $\mathbf{C}_{\ell} = \mathbf{C}_{\ell}^{\text{pre}}\mathbf{C}_{\ell}^{\text{sk}}$  and  $\mathbf{B}_{\ell} = \mathbf{A}_{\ell}^{\text{pre}}\mathbf{B}_{\ell}^{\text{sk}} + \mathbf{B}_{\ell}^{\text{pre}}\mathbf{C}_{\ell}^{\text{sk}}$ . Consequently,

$$\begin{aligned} \sigma_j(\mathbf{A}_{\ell}^{\text{sk}}) &\leq \sigma_{\min}(\mathbf{A}_{\ell}^{\text{pre}})^{-1} \sigma_j(\mathbf{A}_{\ell}^{\text{pre}}\mathbf{A}_{\ell}^{\text{sk}}) = \sigma_{\min}(\mathbf{A}_{\ell}^{\text{pre}})^{-1} \sigma_j(\mathbf{A}_{\ell}) \leq (1 + \delta)\sigma_j(\mathbf{A}_{\ell}), \\ \sigma_j(\mathbf{C}_{\ell}^{\text{sk}}) &\geq \|\mathbf{C}_{\ell}^{\text{pre}}\|_2^{-1} \sigma_j(\mathbf{C}_{\ell}^{\text{pre}}\mathbf{C}_{\ell}^{\text{sk}}) = \|\mathbf{C}_{\ell}^{\text{pre}}\|_2^{-1} \sigma_j(\mathbf{C}_{\ell}) \geq (1 - \delta)^{-1} \sigma_j(\mathbf{C}_{\ell}). \end{aligned}$$

We can combine these inequalities with Eq. (20) to easily get Eqs. (19a) and (19b).

To show Eq. (19c), we first notice that

$$\begin{aligned} \|(\mathbf{A}_{\ell})^{-1}\mathbf{B}_{\ell}\|_2 &= \|(\mathbf{A}_{\ell}^{\text{pre}}\mathbf{A}_{\ell}^{\text{sk}})^{-1}(\mathbf{A}_{\ell}^{\text{pre}}\mathbf{B}_{\ell}^{\text{sk}} + \mathbf{B}_{\ell}^{\text{pre}}\mathbf{C}_{\ell}^{\text{sk}})\|_2 \\ &\leq \|(\mathbf{A}_{\ell}^{\text{sk}})^{-1}\mathbf{B}_{\ell}^{\text{sk}}\|_2 + \|(\mathbf{A}_{\ell}^{\text{sk}})^{-1}(\mathbf{A}_{\ell}^{\text{pre}})^{-1}\mathbf{B}_{\ell}^{\text{pre}}\mathbf{C}_{\ell}^{\text{sk}}\|_2. \end{aligned}$$

In turn, we have

$$\begin{aligned} \|(\mathbf{A}_{\ell}^{\text{sk}})^{-1}(\mathbf{A}_{\ell}^{\text{pre}})^{-1}\mathbf{B}_{\ell}^{\text{pre}}\mathbf{C}_{\ell}^{\text{sk}}\|_2 &\leq \sigma_{\min}(\mathbf{A}_{\ell}^{\text{sk}})^{-1} \sigma_{\min}(\mathbf{R}^{\text{pre}})^{-1} \|\mathbf{R}^{\text{pre}}\|_2 \|\mathbf{C}_{\ell}^{\text{sk}}\|_2 \\ &\leq \left(\frac{1 + \delta}{1 - \delta}\right) \sigma_{\min}(\mathbf{A}_{\ell}^{\text{sk}})^{-1} \|\mathbf{C}_{\ell}^{\text{sk}}\|_2, \end{aligned}$$

which finishes the proof.  $\square$

It is easy to prove Theorems 3 and 4 from here. Start by using Proposition 14 to express the bounds from Proposition 15 in terms of the restricted condition number for  $\mathbf{S}$  on  $\text{range}(\mathbf{M})$ . Straightforward algebra shows that if (2a) and (2b) hold for  $\mathbf{X} = \mathbf{SM}$ , then (19a) and (19b) imply the claim of Theorem 3. Proving Theorem 4 requires a slight detour to show that  $\sigma_{\min}(\mathbf{A}_{\ell}^{\text{sk}})^{-1} \|\mathbf{C}_{\ell}^{\text{sk}}\|_2 \leq f_{\ell}^2$  follows from (19a) and (19b). Combine this new bound with (19c) to see that if (3) holds for  $\mathbf{X} = \mathbf{SM}$  then the claim of Theorem 4 follows.

## B Technical numerical stability results

Here we prove results from Section 3, using notation first defined on page 13.

### B.1 Proof of Lemma 10

The relation Eq. (12) follows directly from [YNYF15]. To show Eq. (11), notice that

$$\|\mathbf{M}_n - \mathbf{Q}_k\mathbf{R}_k\|_{\text{F}} = \|\mathbf{M}_n - \mathbf{M}_k^{\text{pre}}\mathbf{R}_k^{\text{sk}} + \mathbf{E}_1\mathbf{R}_k^{\text{sk}} + \mathbf{Q}_k\mathbf{E}_2\|_{\text{F}}, \quad (23)$$

where  $\mathbf{E}_1 = \mathbf{M}_k^{\text{pre}} - \mathbf{Q}_k \mathbf{R}_k^{\text{pre}}$  and  $\mathbf{E}_2 = \mathbf{R}_k - \mathbf{R}_k^{\text{pre}} \mathbf{R}_k^{\text{sk}}$ . According to [YNYF15], it holds that  $\|\mathbf{E}_1\|_F \leq 8.4 \|\mathbf{M}_k^{\text{pre}}\|_2 n^2 u$ . By combining this relation with Eq. (12) we deduce that  $\|\mathbf{R}_k^{\text{pre}}\|_F \leq 1.01 \|\mathbf{M}_k^{\text{pre}}\|_F$ . Furthermore, by standard rounding bounds for matrix multiplication [Hig02], we have  $\|\mathbf{E}_2\|_F \leq \frac{nu}{1-nu} \|\mathbf{R}_k^{\text{pre}}\|_F \|\mathbf{R}_k^{\text{sk}}\|_F$ . Next, from Eq. (10) it can be deduced that  $\|\mathbf{M}_k^{\text{pre}} \mathbf{R}_k^{\text{sk}}\|_2 \leq 1.01 \|\mathbf{M}\|_2$ , and therefore

$$\|\mathbf{M}_k^{\text{pre}}\|_2 \|\mathbf{R}_k^{\text{sk}}\|_2 \leq 6 \kappa(\mathbf{M}_k^{\text{pre}})^{-1} \|\mathbf{M}_k^{\text{pre}}\|_2 \|\mathbf{R}_k^{\text{sk}}\|_2 \leq 6 \sigma_{\min}(\mathbf{M}_k^{\text{pre}}) \|\mathbf{R}_k^{\text{sk}}\|_2 \leq 6.06 \|\mathbf{M}\|_2.$$

By plugging the obtained bounds for  $\|\mathbf{E}_1\|_F$ ,  $\|\mathbf{R}_k^{\text{pre}}\|_F$ ,  $\|\mathbf{E}_2\|_F$  and  $\|\mathbf{M}_k^{\text{pre}}\|_2 \|\mathbf{R}_k^{\text{sk}}\|_2$  to Eq. (23), we obtain

$$\begin{aligned} \|\mathbf{M}_n - \mathbf{Q}_k \mathbf{R}_k\|_F - \|\mathbf{M}_n - \mathbf{M}_k^{\text{pre}} \mathbf{R}_k^{\text{sk}}\|_F &\leq \|\mathbf{E}_1\|_F \|\mathbf{R}_k^{\text{sk}}\|_2 + \|\mathbf{Q}_k\|_2 \|\mathbf{E}_2\|_F \\ &\leq 8.4 \|\mathbf{M}_k^{\text{pre}}\|_2 n^2 u \|\mathbf{R}_k^{\text{sk}}\|_2 + 1.01 n u \|\mathbf{R}_k^{\text{pre}}\|_F \|\mathbf{R}_k^{\text{sk}}\|_F \\ &\leq 51 n^2 u \|\mathbf{M}\|_2 + 1.03 n u \|\mathbf{M}_k^{\text{pre}}\|_F \|\mathbf{R}_k^{\text{sk}}\|_F \\ &\leq (50.5 n^2 u + 6.3 n^2 u) \|\mathbf{M}\|_2, \end{aligned}$$

which completes the proof.

## B.2 Preconditioner stability

### B.2.1 Assumptions

To characterize numerical stability of CQRRPT's preconditioner, we need assumptions on the accuracy of the operations at Lines 2 to 5 of Algorithm 2 under finite precision arithmetic. We consider a scenario where Line 5, which dominates the preconditioner's computational cost, is computed using unit roundoff  $u$ , whereas cheaper Lines 2 to 4 are computed at a higher precision, using a roundoff  $\tilde{u} = m^{-1} F(n)^{-1} u$ , where  $F(n)$  is a low-degree polynomial. We use this computational model to illustrate a crucial property of the preconditioner: the ability to ensure numerical stability with a roundoff  $u$  for dominant operations independent of  $m$ . This property is of interest for integrating CQRRPT into multi- or low-precision arithmetic architectures. Clearly, the numerical stability of CQRRPT computed with two unit roundoffs also implies its stability when computed with a single roundoff. Define,

$$\begin{aligned} \mathbf{E}_1 &:= \mathbf{S} \mathbf{M}_k - \mathbf{M}_k^{\text{sk}}, \\ \mathbf{E}_2 &:= \mathbf{M}_k^{\text{sk}} - \mathbf{Q}_k^{\text{sk}} \mathbf{R}_k^{\text{sk}} \\ \mathbf{E}_3 &:= \mathbf{M}_k - \mathbf{M}_k^{\text{pre}} \mathbf{A}_k^{\text{sk}} \\ \mathbf{E}_4 &:= \mathbf{S} \bar{\mathbf{M}}_k - \bar{\mathbf{M}}_k^{\text{sk}}, \end{aligned} \tag{24}$$

where  $\bar{\mathbf{M}}_k := \mathbf{M}[:, J[k+1:n]]$  and  $\bar{\mathbf{M}}_k^{\text{sk}} := \mathbf{M}^{\text{sk}}[:, J[k+1:n]]$ .

We require that several bounds hold on these matrices. The choice for these bounds begins with a base assumption that the unit roundoff  $u$  satisfies

$$u \leq 0.001 n^{-\frac{3}{2}} k^{-\frac{5}{2}}. \tag{25a}$$

With that, the first round of bounds that we discuss are

$$\|\mathbf{E}_1[:, j]\|_2 \leq 0.01 k^{-\frac{1}{2}} u \|\mathbf{M}_k[:, j]\|_2 \text{ for } 1 \leq j \leq k, \tag{25b}$$

$$\|\mathbf{E}_2[:, j]\|_2 \leq 0.01 k^{-\frac{1}{2}} u \|\mathbf{M}^{\text{sk}}[:, j]\|_2 \text{ for } 1 \leq j \leq n, \quad \text{and} \quad \|\mathbf{Q}_k^{\text{sk}*} \mathbf{Q}_k^{\text{sk}} - \mathbf{I}\|_F \leq 0.1 u. \tag{25c}$$



It is easy to ensure that these conditions hold. To begin, we note that the classical worst-case rounding analysis ensures  $|\mathbf{E}_1| \leq \frac{m\tilde{u}}{1-m\tilde{u}}|\mathbf{S}||\mathbf{M}_k|$ . This tells us that Eq. (25b) can be achieved if  $\tilde{u} = \mathcal{O}(m^{-1}n^{-1}u)$  and  $\|\mathbf{S}\|_F = \mathcal{O}(\sqrt{m})$ . Meanwhile, the condition Eq. (25c) can be achieved by using any stable QRCP factorization executed in sufficient precision. This for instance includes the Householder QR with unit roundoff  $\tilde{u} = \mathcal{O}(n^{-1}d^{-\frac{3}{2}}u)$  or Givens QR with unit roundoff  $\tilde{u} = \mathcal{O}(n^{-1}d^{-\frac{1}{2}}u)$  [Hig02].

Our next round of assumptions is more substantial. In particular, assume that the output of the black-box `qr` function satisfies the rank-revealing properties

$$\sigma_{\min}(\mathbf{A}_k^{\text{sk}}) \geq 0.5n^{-\frac{1}{2}}k^{-\frac{1}{2}}\sigma_k(\mathbf{M}^{\text{sk}}), \quad \|\mathbf{C}_{k-1}^{\text{sk}}\|_2 \leq 2n^{\frac{1}{2}}k^{\frac{1}{2}}\sigma_k(\mathbf{M}^{\text{sk}}), \quad (25d)$$

$$\|(\mathbf{A}_k^{\text{sk}})^{-1}\mathbf{B}_k^{\text{sk}}\|_F \leq 2n^{\frac{1}{2}}k^{\frac{1}{2}}. \quad (25e)$$

These conditions can be achieved with the strong rank-revealing QR method from [GE96] with unit roundoff  $\tilde{u} = \mathcal{O}(n^{-1}d^{-\frac{1}{2}}u)$ . The method from [GE96] contains an extra parameter  $f$  that in our case should be taken as, say, 1.5. Then the `qr` subroutine on Line 3 will take a negligible amount  $\mathcal{O}(dn^2 \log n)$  of flops and satisfy Eqs. (25d) and (25e). It is important to note that in practical applications, the condition Eqs. (25d) and (25e) is expected to hold also for traditional QRCP with max-norm column pivoting. However, there are a few exceptional cases in which the traditional QRCP would not satisfy Eq. (25e).

Next, according to [Hig02, Theorem 8.5], we have  $\mathbf{M}_k^{\text{pre}}[j, :](\mathbf{A}_k^{\text{sk}} + \Delta\mathbf{A}^{(j)}) = \mathbf{M}_k[j, :]$  with  $|\Delta\mathbf{A}^{(j)}| \leq 1.1uk|\mathbf{A}_k^{\text{sk}}|$ , which implies that  $|\mathbf{E}_3|$  is bounded by  $1.1uk|\mathbf{M}_k^{\text{pre}}||\mathbf{A}_k^{\text{sk}}|$  and leads to the following condition

$$|\mathbf{E}_3[:, j]| \leq 1.1ku|\mathbf{M}_k^{\text{pre}}||\mathbf{A}_k^{\text{sk}}[:, j]| \text{ for } 1 \leq j \leq k. \quad (25f)$$

Furthermore, by the standard rounding analysis we have  $|\mathbf{E}_4| \leq \frac{m\tilde{u}}{1-m\tilde{u}}|\mathbf{S}||\bar{\mathbf{M}}_k|$ , which implies

$$\|\mathbf{E}_4[:, j]\|_2 \leq 0.1n^{-\frac{1}{2}}u\|\bar{\mathbf{M}}_k[:, j]\|_2 \text{ for } 1 \leq j \leq n-k, \quad (25g)$$

if  $\tilde{u} = \mathcal{O}(m^{-1}n^{-1}u)$  and  $\|\mathbf{S}\|_F = \mathcal{O}(\sqrt{m})$ .

With the computational model based on the assumptions Eq. (25), we can now establish a numerical characterization of the CQRRPT preconditioner.

## B.2.2 Main result

Theorem 16 is our main numerical stability result. It guarantees stability of CQRRPT's preconditioner under the condition that the truncation error associated with the preceding index  $k-1$  is greater than the threshold value  $G(n, k)u$ , where  $G(n, k)$  is a low-degree polynomial. Consequently, by using the largest  $k$  that satisfies this condition, we will have a factorization  $\mathbf{M}_k^{\text{pre}}\mathbf{R}_k^{\text{sk}}$ , which is within a distance of  $G(n, k)u$  from  $\mathbf{M}_n$  and for which  $\mathbf{M}_k^{\text{pre}}$  is well-conditioned.

**Theorem 16.** *Consider Algorithm 2 where Line 5 is executed with unit roundoff  $u \leq 0.001n^{-\frac{3}{2}}k^{-\frac{5}{2}}$ . Assume that the other lines are executed with unit roundoff  $\tilde{u} = m^{-1}F(n)^{-1}u$ , where  $F(n)$  is some low-degree polynomial, and  $\|\mathbf{S}\|_F = \mathcal{O}(\sqrt{m})$ , so that the conditions Eq. (25) hold. Assume that  $k$  satisfies*

$$1000n^{\frac{3}{2}}k^{\frac{5}{2}}u \leq \frac{\|\mathbf{C}_{k-1}^{\text{sk}}\|_F}{\|\mathbf{R}_k^{\text{sk}}\|_2}.$$

If  $\mathbf{S}$  is an  $\delta$ -embedding for  $\text{range}(\mathbf{M})$  with  $\delta \leq \frac{1}{4}$ , then

$$\frac{\|\mathbf{M}_n - \mathbf{M}_k^{\text{pre}} \mathbf{R}_k^{\text{sk}}\|_{\text{F}}}{\|\mathbf{M}\|_{\text{F}}} \leq 2 \frac{\|\mathbf{C}_k^{\text{sk}}\|_{\text{F}}}{\|\mathbf{R}_k^{\text{sk}}\|_2} + 10nku \quad (26a)$$

$$0.8 \leq \sigma_{\min}(\mathbf{M}_k^{\text{pre}}) \leq \sigma_{\max}(\mathbf{M}_k^{\text{pre}}) \leq 1.44. \quad (26b)$$

Theorem 16 can be reformulated to incorporate the effective distortion of  $\mathbf{S}$ , as below.

**Corollary 17.** Let  $\mathbf{M}$ ,  $\mathbf{u}$ ,  $\tilde{\mathbf{u}}$ ,  $k$  be as in Theorem 16. If for some  $t$ ,  $t\mathbf{S}$  is an  $\delta$ -embedding for  $\mathbf{M}$  with  $\delta \leq \frac{1}{4}$  and  $t\|\mathbf{S}\|_{\text{F}} = \mathcal{O}(\sqrt{m})$ , then we have

$$\frac{\|\mathbf{M}[:, J] - \mathbf{M}_k^{\text{pre}} \mathbf{R}_k^{\text{sk}}\|_{\text{F}}}{\|\mathbf{M}\|_{\text{F}}} \leq 2 \frac{\|\mathbf{C}_k^{\text{sk}}\|_{\text{F}}}{\|\mathbf{R}_k^{\text{sk}}\|_2} + 10nku \quad \text{and} \quad \kappa(\mathbf{M}_k^{\text{pre}}) \leq 1.8.$$

*Proof.* Notice that the following substitution

$$\mathbf{S} \leftarrow t\mathbf{S}, \mathbf{M}^{\text{sk}} \leftarrow t\mathbf{M}^{\text{sk}}, \mathbf{Q}_k^{\text{sk}} \leftarrow \mathbf{Q}_k^{\text{sk}}, \mathbf{R}_k^{\text{sk}} \leftarrow t\mathbf{R}_k^{\text{sk}}, \text{ and } \mathbf{M}^{\text{pre}} \leftarrow t^{-1}\mathbf{M}^{\text{pre}} \quad (28)$$

will not affect assumptions Eq. (25) and the condition  $1000n^{\frac{3}{2}}k^{\frac{5}{2}}\mathbf{u} \leq \|\mathbf{C}_{k-1}^{\text{sk}}\|_{\text{F}}\|\mathbf{R}_k^{\text{sk}}\|_2^{-1}$  of Theorem 16. The result of the corollary then follows directly from Theorem 16.  $\square$

Our proof of Theorem 16 uses two intermediate propositions that provide further insights into the stability of the CQRRPT preconditioner. First, Proposition 18 concerns how the permutation obtained on Line 3 of CQRRPT effectively bounds the condition number of the submatrix  $\mathbf{M}_k$ . Second, Proposition 19 involves examining the factors  $\mathbf{M}_k^{\text{pre}}$  and  $\mathbf{A}_k^{\text{sk}}$  as an unpivoted “sketched CholeskyQR” factorization of  $\mathbf{M}_k$ , which enables us to leverage a result from [Bal22].

**Proposition 18.** Consider Algorithm 2 where Line 5 is executed with unit roundoff  $\mathbf{u} \leq 0.001n^{-\frac{3}{2}}k^{-\frac{5}{2}}$  and other lines are executed with unit roundoff  $\tilde{\mathbf{u}} = m^{-1}F(n)^{-1}\mathbf{u}$ , where  $F(n)$  is some low-degree polynomial, and  $\|\mathbf{S}\|_{\text{F}} = \mathcal{O}(\sqrt{m})$ , so that the conditions Eq. (25) hold. Assume that  $k$  is such that

$$n^{\frac{3}{2}}k\mathbf{u} \leq \|\mathbf{C}_{k-1}^{\text{sk}}\|_{\text{F}}\|\mathbf{R}_k^{\text{sk}}\|_2^{-1}.$$

If  $\mathbf{S}$  is an  $\delta$ -embedding for  $\mathbf{M}_k$  with  $\delta \leq \frac{1}{4}$ , then we have

$$\kappa(\mathbf{M}_k) \leq 10n^{\frac{3}{2}}k\|\mathbf{C}_{k-1}^{\text{sk}}\|_{\text{F}}^{-1}\|\mathbf{R}_k^{\text{sk}}\|_2 \leq 2.5\mathbf{u}^{-1}.$$

*Proof.* Denote  $\|\mathbf{C}_{k-1}^{\text{sk}}\|_{\text{F}}\|\mathbf{R}_k^{\text{sk}}\|_2^{-1}$  by  $\tau_{k-1}$ . Frame the assumptions Eq. (25). Notice that by Eq. (25d),

$$\sigma_{\min}(\mathbf{A}_k^{\text{sk}}) \geq 4^{-1}n^{-1}k^{-1}\|\mathbf{C}_{k-1}^{\text{sk}}\|_2 \geq 4^{-1}n^{-\frac{3}{2}}k^{-1}\tau_{k-1}\|\mathbf{A}_k^{\text{sk}}\|_2. \quad (29)$$

Thus, it is deduced that

$$\kappa(\mathbf{A}_k^{\text{sk}}) \leq 4n^{\frac{3}{2}}k\tau_{k-1}^{-1} \leq \mathbf{u}^{-1}. \quad (30)$$

Furthermore, by Eq. (25c) we have

$$\|\mathbf{M}_k^{\text{sk}}\|_2 \leq \|\mathbf{Q}_k^{\text{sk}}\|_2\|\mathbf{A}_k^{\text{sk}}\|_2 + \|\mathbf{E}_2[:, 1:k]\|_2 \leq 1.01\|\mathbf{A}_k^{\text{sk}}\|_2, \quad (31)$$

and

$$\begin{aligned} \sigma_{\min}(\mathbf{M}_k^{\text{sk}}) &\geq \sigma_{\min}(\mathbf{Q}_k^{\text{sk}})\sigma_{\min}(\mathbf{A}_k^{\text{sk}}) - \|\mathbf{E}_2[:, 1:k]\|_2 \\ &\geq 0.99\sigma_{\min}(\mathbf{A}_k^{\text{sk}}) - 0.01\mathbf{u}\|\mathbf{M}_k^{\text{sk}}\|_2 \geq 0.99\sigma_{\min}(\mathbf{A}_k^{\text{sk}}) - 0.011\mathbf{u}\|\mathbf{A}_k^{\text{sk}}\|_2 \\ &\geq \sigma_{\min}(\mathbf{A}_k^{\text{sk}})(0.99 - 0.011\mathbf{u}\kappa(\mathbf{A}_k^{\text{sk}})) \geq 0.97\sigma_{\min}(\mathbf{A}_k^{\text{sk}}). \end{aligned} \quad (32)$$

Consequently,

$$\kappa(\mathbf{M}_k^{\text{sk}}) \leq 4.2n^{\frac{3}{2}}k\tau_{k-1}^{-1} \leq 1.05u^{-1}. \quad (33)$$

Next, by Eq. (25b) we get

$$\|\mathbf{S}\mathbf{M}_k\|_2 \leq \|\mathbf{M}_k^{\text{sk}}\|_2 + \|\mathbf{E}_1\|_2 \leq 1.01\|\mathbf{M}_k^{\text{sk}}\|_2, \quad (34)$$

which due to the  $\delta$ -embedding property of  $\mathbf{S}$  implies that

$$\|\mathbf{M}_k\|_2 \leq 1.5\|\mathbf{M}_k^{\text{sk}}\|_2. \quad (35)$$

We also have by Eqs. (25b) and (33),

$$\begin{aligned} \sigma_{\min}(\mathbf{S}\mathbf{M}_k) &\geq \sigma_{\min}(\mathbf{M}_k^{\text{sk}}) - \|\mathbf{E}_1\|_2 \geq \sigma_{\min}(\mathbf{M}_k^{\text{sk}}) - 0.01u\|\mathbf{M}_k\|_2 \\ &\geq \sigma_{\min}(\mathbf{M}_k^{\text{sk}}) - 0.015u\|\mathbf{M}_k^{\text{sk}}\|_2 \geq 0.92\sigma_{\min}(\mathbf{M}_k^{\text{sk}}). \end{aligned} \quad (36)$$

Consequently, by the  $\delta$ -embedding property of  $\mathbf{S}$  and Eqs. (35) and (36),

$$\kappa(\mathbf{M}_k) \leq \frac{1+\delta}{1-\delta} \kappa(\mathbf{S}\mathbf{M}_k) \leq 1.91 \kappa(\mathbf{M}_k^{\text{sk}}) \leq 10n^{\frac{3}{2}}k\tau_{k-1}^{-1} \leq 2.5u^{-1},$$

which finishes the proof.  $\square$

**Proposition 19** (Corollary of Theorem 5.2 from [Bal22]). *Consider Algorithm 2 where Line 5 is executed with unit roundoff  $u \leq 0.01n^{-\frac{3}{2}} \kappa(\mathbf{M}_k)^{-1}$  and other lines are executed with unit roundoff  $\tilde{u} = m^{-1}F(k)^{-1}u$ , where  $F(k)$  is some low-degree polynomial, and  $\|\mathbf{S}\|_{\text{F}} = \mathcal{O}(\sqrt{m})$ , so that the assumptions Eq. (25) hold. If  $\mathbf{S}$  is an  $\delta$ -embedding for  $\mathbf{M}_k$  with  $\delta \leq \frac{1}{4}$  then*

$$\mathbf{M}_k + \Delta\mathbf{M} = \mathbf{M}_k^{\text{pre}} \mathbf{A}_k^{\text{sk}} \quad (37)$$

with  $\|\Delta\mathbf{M}_k[:, j]\|_2 \leq 2.1ku\|\mathbf{M}[:, j]\|_2$  for  $1 \leq j \leq k$ . Furthermore, we have

$$(1+\delta)^{-1} - 4k^{\frac{3}{2}}u\kappa(\mathbf{M}_k) \leq \sigma_{\min}(\mathbf{M}_k^{\text{pre}}) \leq \sigma_{\max}(\mathbf{M}_k^{\text{pre}}) \leq (1-\delta)^{-1} + 4k^{\frac{3}{2}}u\kappa(\mathbf{M}_k). \quad (38)$$

We are now ready to present the proof of Theorem 16.

*Proof of Theorem 16.* Denote  $\|\mathbf{C}_k^{\text{sk}}\|_{\text{F}}\|\mathbf{R}_k^{\text{sk}}\|_2^{-1}$  by  $\tau_k$ . By Eqs. (25b), (25c), (25e) and (25g) we have

$$\begin{aligned} \|\bar{\mathbf{M}}_k - \mathbf{M}_k^{\text{pre}} \mathbf{B}_k^{\text{sk}}\|_{\text{F}} &\leq \|\bar{\mathbf{M}}_k - \mathbf{M}_k(\mathbf{A}_k^{\text{sk}})^{-1} \mathbf{B}_k^{\text{sk}}\|_{\text{F}} + \|\mathbf{E}_3(\mathbf{A}_k^{\text{sk}})^{-1} \mathbf{B}_k^{\text{sk}}\|_{\text{F}} \\ &\leq (1-\delta)^{-1} \|\mathbf{S}(\bar{\mathbf{M}}_k - \mathbf{M}_k(\mathbf{A}_k^{\text{sk}})^{-1} \mathbf{B}_k^{\text{sk}})\|_{\text{F}} + \|\mathbf{E}_3\|_{\text{F}} \|(\mathbf{A}_k^{\text{sk}})^{-1} \mathbf{B}_k^{\text{sk}}\|_2 \\ &\leq (1-\delta)^{-1} (\|\mathbf{E}_4 + \mathbf{E}_5 + \mathbf{E}_6 + \mathbf{E}_7\|_{\text{F}}) + 2n^{\frac{1}{2}}k^{\frac{1}{2}}\|\mathbf{E}_3\|_{\text{F}}, \end{aligned} \quad (39)$$

where

$$\begin{aligned} \|\mathbf{E}_4\|_{\text{F}} &= \|\mathbf{S}\bar{\mathbf{M}}_k - \bar{\mathbf{M}}_k^{\text{sk}}\|_{\text{F}} \leq 0.1u\|\bar{\mathbf{M}}_k\|_2 \\ \|\mathbf{E}_5\|_{\text{F}} &= \|\bar{\mathbf{M}}_k^{\text{sk}} - \mathbf{Q}_k^{\text{sk}} \mathbf{B}_k^{\text{sk}}\|_{\text{F}} \leq \|\mathbf{Q}_k^{\text{sk}}\|_2 \|\mathbf{C}_k^{\text{sk}}\|_{\text{F}} + \|\mathbf{E}_2\|_{\text{F}} \\ &\leq 1.01\tau_k \|\mathbf{R}_k^{\text{sk}}\|_2 + \|\mathbf{E}_2\|_{\text{F}} \leq (1+\delta)(1.02\tau_k + 0.01\sqrt{nu})\|\mathbf{M}\|_{\text{F}} \\ \|\mathbf{E}_6\|_{\text{F}} &= \|(\mathbf{Q}_k^{\text{sk}} \mathbf{A}_k^{\text{sk}} - \mathbf{M}_k^{\text{sk}})(\mathbf{A}_k^{\text{sk}})^{-1} \mathbf{B}_k^{\text{sk}}\|_{\text{F}} \\ &\leq \|\mathbf{Q}_k^{\text{sk}} \mathbf{A}_k^{\text{sk}} - \mathbf{M}_k^{\text{sk}}\|_{\text{F}} \|(\mathbf{A}_k^{\text{sk}})^{-1} \mathbf{B}_k^{\text{sk}}\|_2 \\ &\leq 2n^{\frac{1}{2}}k^{\frac{1}{2}}\|\mathbf{E}_2[:, 1:k]\|_{\text{F}} \leq 0.02n^{\frac{1}{2}}k^{\frac{1}{2}}u\|\mathbf{M}_k^{\text{sk}}\|_2 \leq 0.03nu\|\mathbf{M}_k\|_2 \\ \|\mathbf{E}_7\|_{\text{F}} &= \|(\mathbf{M}_k^{\text{sk}} - \mathbf{S}\mathbf{M}_k)(\mathbf{A}_k^{\text{sk}})^{-1} \mathbf{B}_k^{\text{sk}}\|_2 \leq \|\mathbf{M}_k^{\text{sk}} - \mathbf{S}\mathbf{M}_k\|_{\text{F}} \|(\mathbf{A}_k^{\text{sk}})^{-1} \mathbf{B}_k^{\text{sk}}\|_2 \\ &\leq 2n^{\frac{1}{2}}k^{\frac{1}{2}}\|\mathbf{E}_1\|_{\text{F}} \leq 0.02nu\|\mathbf{M}_k\|_2. \end{aligned}$$

By using the triangle inequality and the fact that  $\delta \leq \frac{1}{4}$ , we obtain

$$\|\bar{\mathbf{M}}_k - \mathbf{M}_k^{\text{pre}} \mathbf{B}_k^{\text{sk}}\|_{\text{F}} \leq \frac{4}{3}(0.2n\mathbf{u} + 1.02\frac{5}{4}\tau_k)\|\mathbf{M}\|_{\text{F}} + 2n^{\frac{1}{2}}k^{\frac{1}{2}}\|\mathbf{E}_3\|_{\text{F}}. \quad (40)$$

Furthermore, from Proposition 18 it follows that

$$\kappa(\mathbf{M}_k) \leq 10n^{\frac{3}{2}}k\tau_k^{-1}. \quad (41)$$

By looking at  $\mathbf{M}_k^{\text{pre}}$  and  $\mathbf{A}_k^{\text{sk}}$  as a sketched CholeskyQR factorization of  $\mathbf{M}_k$ , according to Proposition 19, we have

$$\|\mathbf{E}_3\|_{\text{F}} = \|\mathbf{M}_k - \mathbf{M}_k^{\text{pre}} \mathbf{A}_k^{\text{sk}}\|_{\text{F}} \leq 2.1k\mathbf{u}\|\mathbf{M}_k\|_{\text{F}} \quad (42a)$$

$$(1 + \delta)^{-1} - 4k^{\frac{3}{2}}\mathbf{u}\kappa(\mathbf{M}_k) \leq \sigma_{\min}(\mathbf{M}_k^{\text{pre}}) \leq \sigma_{\max}(\mathbf{M}_k^{\text{pre}}) \leq (1 - \delta)^{-1} + 4k^{\frac{3}{2}}\mathbf{u}\kappa(\mathbf{M}_k) \quad (42b)$$

By combining Eq. (42a) with Eq. (40) and using the triangle inequality we obtain Eq. (26a). By combining Eq. (42b) with Eq. (41) we obtain Eq. (26b) and finish the proof.  $\square$

## C More on numerical experiments

### C.1 Benchmarking with very tall matrices

The matrices used in Section 5's experiments were tall, but not as tall as some readers might anticipate. Therefore here we consider matrices with one million rows and  $32 \dots 16384$  columns. Figure 9 presents performance results (in canonical GFLOPs/second) for the algorithms considered before. It shows that for very thin matrices ( $n \leq 256$ ), CQRRPT may be inefficient compared to alternative algorithms. This can be understood with performance profiling data in Figure 10. Specifically, for these extremely tall and thin matrices the runtime is dominated by sketching, and the time to pivot  $\mathbf{M}$  before preconditioning takes nearly as long as CholeskyQR. As before, our experiments were run on the machine described in Table 1 using 48 threads.

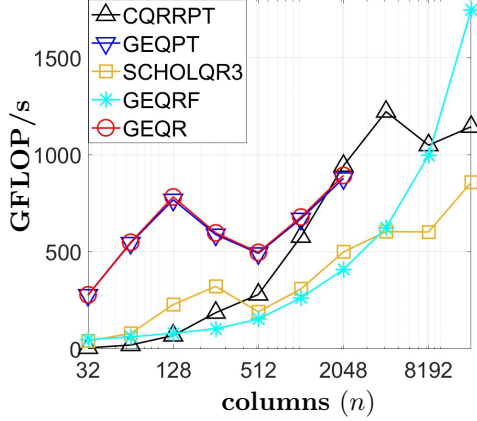


Figure 9: QR schemes performance comparisons for matrices with one million rows and varying numbers of columns (32, ..., 16384). The plot does not depict GEQR and GEQPT results for the number of columns larger than 2048, as we encountered memory errors with running Intel MKL’s GEQR for such sizes.

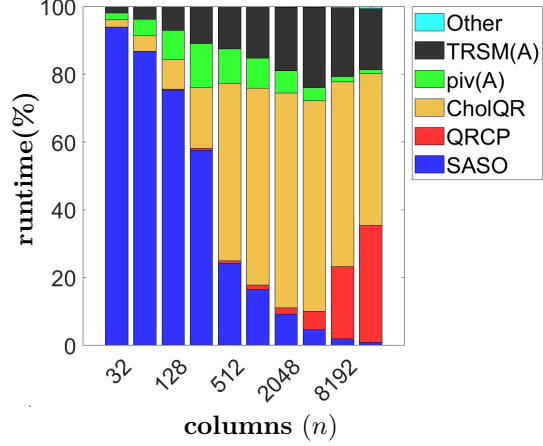


Figure 10: Percentages of runtime used by CQRRPT’s subroutines, for matrices with one million rows and the indicated number of columns. Note that although CholQR occupies the dominant portion of runtime across the larger ( $n \geq 512$ ) matrix sizes, its runtime is primarily comprised of vector-vector operations for the smaller matrix sizes. As the matrix size increases, TRSM routine gradually achieves a GEMM-like performance level.

## C.2 HQRRP performance details

Figure 8 is our attempt to give a contemporary refresh of Figures 4 and 5 from the original HQRRP publication [MQOHvdG17]. It is important to note that the initial HQRRP thread scalability study was performed on Intel Xeon E5-2695v3 (the Haswell platform) processor with clocked capped at 2.3 GHz featuring “only” 14 cores in a single socket with 22nm node size. Our experiments used dual-socket Intel Xeon Gold 6248R (Cascade Lake platform) with 24 cores per socket and 48 cores total with 14nm feature size – a NUMA design. In essence, the new processor engages a much larger numbers of cores in the computation and they have to be coordinated by on-node interconnect, that is, the design keeps the content of Level 1 caches coherent through a memory controller state tracking each L1 cache line. At every iteration, HQRRP forms a random projection to select the pivots and this relatively small matrix becomes the target of contention between the cores. Accessing its elements overwhelms the cache coherency protocol that has to redistribute the projection data so that the cores can proceed to perform independent work. Thus, we observe Figure 8 that the performance drops for larger core counts as the contention increases. For smaller matrix sizes, lower-level caches, especially Level 3, are very effective in alleviating the demand for cache lines from the main memory and HQRRP behaves as it did on the old Haswell system.